5.18 Molten Salt Reactor Fuel and Coolant[☆]

Ondřej Beneš and Rudy JM Konings, European Commission, Joint Research Centre, Karlsruhe, Germany

[☆]*Change History*: February 2020. Ondřej Beneš and Rudy Konings updated the Chapter on key chloride systems with focus on structural aspect, physico-chemical properties and electrochemical properties. Next experimental data on selected MSR fuel systems obtained in the last decay are included in this version. Chapter includes information about current MSR concepts which evolved in the past few years, both national and vendor's concepts. Key challenges for MSR deployment are included in the chapter.
This is an update of Beneš, O., Konings, R.J.M., 2012. Chapter 3.13 – Molten Salt Reactor Fuel and Coolant. In: Konings, R.J.M. (Ed.), Comprehensive Nuclear Materials, Elsevier, pp. 359–389.

5.18.1 Introduction

The molten salt reactor (MSR) is one of the six reactor concepts of the Generation IV initiative, which is an international collaboration to study the next generation nuclear power reactors. The fuel of the MSR is based on the dissolution of the fissile material (^{235}U, ^{233}U, or ^{239}Pu) in an inorganic liquid that is pumped at a low pressure through the reactor vessel and the primary circuit, and thus also serves as the primary coolant. The heat generated by the fission process is transferred in a heat exchanger to a secondary coolant, which is also generally a molten salt. This intermediate loop is introduced for safety reasons: to avoid direct contact between the steam and the fuel. A schematic drawing of the MSR is shown in **Fig. 1(a)** as taken from US DOE Roadmap.[1]

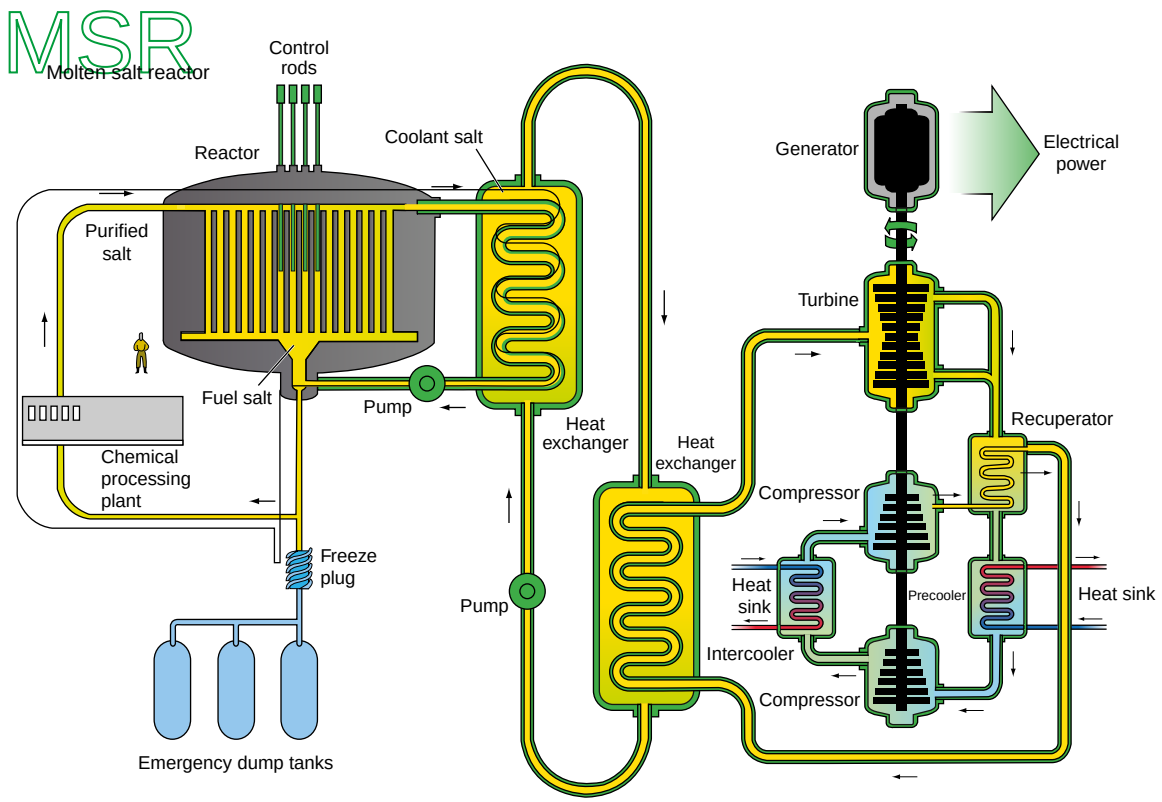

Fig. 1 (a) Schematic drawing of the molten salt reactor. (b) Overview of MSR concepts studied nowadays (see next page). Reproduced from US DOE Nuclear Energy Research Advisory Committee and the Generation IV International Forum, 2002. A Technology Roadmap for Generation IV Nuclear Energy Systems. Available at: https://www.gen-4.org/gif/jcms/c_40481/technology-roadmap. Anon1, 2017. GIF Annual Report.

Thermal Spectrum Liquid Fuel MSRs			
Thorium Molten Salt Reactor, Liquid Fuel (TMSR-LF)	Shanghai Institute of Applied Physics (SINAP), China	395	ThF_4-$^{233}UF_4$/^{7}LiF-BeF_2/graphite
Integral Molten Salt Reactor (IMSR)	Terrestrial Energy, Canada and the United States	400	UF_4/fluorides/graphite
ThorCon Reactor	ThorCon International, Singapore	557×2	UF_4/NaF-BeF_2/graphite
Liquid-Fluoride Thorium Reactor (LFTR)	Flibe Energy, United States	600	ThF_4-$^{233}UF_4$/^{7}LiF-BeF_2/graphite
FUJI-U3	Japan	450	ThF_4-$^{233}UF_4$/^{7}LiF-BeF_2/graphite
Advanced Molten-salt Break-even Inherently-safe Dual-mission Experimental and Test Reactor (AMBIDEXTER)	Ajou University, Korea	250	$^{233}UF_4$-ThF_4/^{7}LiF-BeF_2
Transatomic Power MSR (TAP)	Transatomic Power, United States	1 250	UF_4/FLiNaK/SiC clad $ZrH_{1.6}$
Compact Used fuel BurnEr (CUBE)	Seaborg Technologies, Denmark	250	SNF/fluorides/graphite
Process Heat Reactor	Thorenco, United States	50	UF_4/NaF-BeF_2,/Be rods
Stable Salt Thermal Reactor (SSR-U)	Moltex Energy, United Kingdom	300-2 500	UF_4/fluorides/graphite
Fast/Epithermal Spectrum Liquid Fuel MSRs			
Molten Salt Fast Reactor (MSFR)	SAMOFAR, France – EU – Switzerland	3 000	ThF_4-UF_4/^{7}LiF-
Molten Salt Actinide Recycler and Transformer (MOSART)	Kurchatov Institute, Russia	2 400	$TRUF_3$ or ThF_4-UF_4/^{7}LiF-BeF_2 or NaF-^{7}LiF-BeF_2
U-Pu Fast Molten Salt Reactor (U-Pu FMSR)	VNIINM, Russia	3 200	UF_4-PuF_3/^{7}LiF-NaF-KF
Indian Molten Salt Breeder Reactor (IMSBR)	BARC, India	1 900	ThF_4-UF_4/LiF-
Stable Salt Fast Reactor (SSR-W)	Moltex Energy, United Kingdom	750-2 500	PuF_3/Fluorides
Molten Chloride Fast spectrum Reactor (MCFR)	TerraPower, United States		U-Pu/Chlorides
Molten Chloride Salt Fast Reactor (MCSFR)	Elysium Industries, United States and Canada	100-5 000	U-Pu/Chlorides
Dual Fluid Reactor (DFR)	Dual Fluid Reactor, Germany	3 000	U-Pu/Chlorides
Solid Fuel MSRs (all thermal spectrum)			
Molten-Salt Reactor with Micro-Particle Fuel (MARS)	Kurchatov Institute, Russia	16	TRISO-coated LEU/FLiBe/Graphite pebble bed
Advanced High Temperature Reactor (AHTR)	ORNL, United States	3 400	Coated U particles in blocks or plates/FLiBe/Graphite
Small Advanced High Temperature Reactors (SmAHTR)	ORNL, United States	125	Coated U particles in blocks or plates/FLiBe/Graphite
Pebble Bed – Fluoride Salt-Cooled High Temperature Reactors (PB-FHR)	UC Berkeley, MIT and UW, United States	242	TRISO-coated LEU/FLiBe/Graphite pebble bed
Thorium Molten Salt Reactor, Solid Fuel (TMSR-SF)	SINAP, China	395	TRISO-coated U-Th/FLiBe/Graphite pebble bed
Indian High Temperature Reactor (IHTR)	BARC, India	600	TRISO-coated U-Th/FLiBe/Graphite pebble bed

Fig. 1 Continued.

Table 1 Typical fuel salt inlet temperatures of selected MSR concepts

MSR concept	T_{inlet}	T_{outlet}	*Reference*
MSRE	908K	936K	2
MSBR	839K	977K	3
MSFR	903K	923K	4
MOSART	873K	988K	5
TMSR	873K	923K	

The operating temperature of the MSR is between 800 and 1000K, the lower limit being determined by the fusion temperature of the salt and the upper one by the corrosion rate of the structural material. Typical inlet and outlet temperatures of some MSR concepts, which are briefly discussed in Section 5.18.3, are summarized in **Table 1**. It is worth mentioning that at least a 50K safety margin must be kept in all concepts, and hence the melting temperature of the fuel salt should be reasonably (< 50K) lower than the designed inlet temperature of the reactor. The fact that the fuel of the MSR is in the liquid state offers several advantages. The first among them is the safety of the reactor. As the fuel is in the liquid state and serves as primary coolant having low vapor pressures (boiling points $>1400^{\circ}$C), the total pressure of the primary circuit is kept very low ($p \sim 1$ bar) compared to, for example, current light water reactors. It thus avoids the major driving force, the high pressure, for radioactivity release during accidents. Another aspect that contributes to the safety of the MSR is that the reactor possesses a strong negative temperature coefficient, so the chain reaction automatically slows down when the temperature increases. This is induced by the thermal expansion of the primary coolant, which pushes the fuel out of the reactor core (the fuel density decreases). The third characteristic that increases the safety of the reactor is the possibility of draining the liquid fuel into emergency dump tanks in case of an accident. The emergency tanks are installed under the reactor and are designed in such way that the fuel remains in a subcritical state.

Another big advantage of the MSR is the possibility of performing a continuous fuel cleanup, which results in an increase of the fuel burnup. This chemical cleanup can be done either online or in batches. The goal of the fuel cleanup is to separate the fission products from the fuel and transfer them into the nuclear waste, while the cleaned fuel is sent back into the primary circuit. It is very important to make this separation because most of the fission products have a very high neutron capture cross-section and thus slow down the chain reaction. Because of the online cleanup, a very low amount of fission products is present in the fuel during the reactor operation, and thus the heat generation from their radioactive decay is small and the risk of overheating in the event of loss of cooling is avoided. Moreover, it is also possible to profit from the neutron economy and design the MSR as a breeder reactor that produces more fuel than it consumes, for example, using a ^{232}Th/^{233}U cycle.

Furthermore, because of the liquid state of the MSR fuel, there is no radiation damage to the fuel (as discussed in Section 5.18.7). Therefore, issues such as swelling or crack formation that appear in the case of ceramic fabricated fuels are avoided. Nevertheless, once the fuel cools down, e.g., during the reactor shut down or storage, the radiological decomposition becomes an issue leading to formation of fluorine gas and preventive measures must be made to avoid such event. More to this topic is addressed in Section 5.18.7 of this article.

As described above, the MSR technology provides many safety related and/or potential economic benefits, but there are still many challenges that need to be addressed before final commercialization of the technology.

Among the first ones is the compatibility of the fuel salt with structural materials at high (operating) temperature and related development of alloys that are resistant enough under these conditions. Dedicated information on corrosion and related redox control of the salt is given in Section 5.18.7 of this article, indicating options how to inhibit corrosion rate, but further research must be still done in this domain to go towards licensing and qualification of novel and compatible alloys.

Another challenge is the establishment of a full procedure of the fuel clean-up scheme, in the case MSR will be coupled with a chemical plant. Although several methods and sequence of physico-chemical steps are proposed at the moment, significant research and validation must be done to properly design an effective scheme with properly installed safeguards and utilizing safe handling of separated fission products.

In case the MSR fuel salt is based on a lithium fluoride containing matrix, issues with tritium production must be taken into account and very likely only coolant salts with high tritium retention can be used as secondary coolant medium.

The last, but not the least identified challenge is the need for reliable data on relevant physico-chemical properties which can be used by authorities for licensing of the reactor. A list of properties of concern is discussed throughout this article. It is not only important to address fuel properties, but also to assess how might these properties be affected by small composition changes caused by factors such as long lasting fission and related fission products build-up, etc.

5.18.2 Historical Background

In the past molten salt reactor technology has been widely studied and promoted in many countries around the world; in the United States, UK, China, Russia, Switzerland, France and India, but since only in the United States the technology was mature enough to make a MSR critical, this section mainly focuses on these major historical achievements with brief description of key concepts.

The first proposal for a MSR dates back to the 1940s when Bettis and Briant proposed it for aircraft propulsion.[6] A substantial research program was initiated at ORNL in the USA to develop this concept, culminating in the Aircraft Reactor Experiment (ARE) which became critical in 1954. The ARE was operated successfully over a period of 221 h at steady-state with outlet temperatures

up to 860°C and at powers up to 2.5 MWth. The ARE used molten fluoride salt with NaF–ZrF_4–UF_4 (53–41–6 mol%) as an initial fuel mixture for the following reasons[7,8]:

(1) Wide range of solubility for thorium and uranium.
(2) Thermodynamic stability up to high temperatures.
(3) No radiolytic decomposition.
(4) Low vapor pressure at the operating temperature of the reactor.
(5) Compatibility with nickel-based alloys (Ni–Mo–Cr–Fe) that can be used as structural materials.

The ARE reactor core was moderated by beryllium oxide (BeO), and it used liquid sodium as a secondary coolant material.[6] In this experiment Inconel 600 alloy (a nickel-based alloy) was used for the metal structure and piping. ARE showed that the fissile compound UF_4 was chemically stable in the solvent and that gaseous fission products were removed automatically by the pumping action of the salt circulation pump. The fluid fuel had a very strong negative temperature coefficient which made the reactor inherently safe. Although the ARE experiment proved the reactor concept, no airplane with such propulsion has ever been constructed.

By the end of the 1950s, the molten salt technology was transferred to the civilian nuclear program in the US. At the time, many reactor concepts were being studied and the interest in breeder reactors was growing. It was recognized that the MSR would be ideal for thermal breeding of uranium from thorium,[9] and the Molten Salt Reactor Experiment (MSRE) was initiated at ORNL to demonstrate the operability of MSRs. Because of the breeding aspect of this design, the neutron economy in the reactor was considered to be of key importance, and ^{7}LiF–BeF_2 (commonly referred to as "FLIBE"), with 5% ZrF_4 as oxygen getter, was selected as fuel carrier because of the very low neutron capture cross-sections of ^{7}Li ($\sigma_{thermal}=0.045$ barn) and Be ($\sigma_{thermal}=0.0088$ barn). Natural lithium could not be used as part of the nuclear fuel as it contains about 7.6% of ^{6}Li (the remaining 92.4% is ^{7}Li), which has a very high parasitic neutron capture cross-section ($\sigma_{thermal}=940$ barn). Therefore, to achieve net positive breeding an enrichment of ^{7}Li was. The MSRE was a graphite-moderated reactor of 8 MWth power and operated from 1965 to 1969. Two different fissile sources were used: initially, $^{235}UF_4$ was used with 33% enrichment and later, $^{233}UF_4$ was added to the carrier salt, making the MSRE the world's first reactor to be fueled with this fissile material.[10] FLIBE was used as coolant in the secondary circuit. The results of MSRE, which have been reported in great detail by Haubenreich *et al.*,[10] revealed that all the selected materials (e.g., fuel mixture, structural materials, etc.) all performed well and that the equipment was considered as reliable technology. In this respect the MSRE project was concluded as very successful.

Following the success of the MSRE project, a design for a prototype molten salt breeder reactor (MSBR) was made by ORNL in the early 1970s,[3] in which a continuous clean-up of the fuel was foreseen to reduce the neutron loss by capture in fission products. The program was terminated in 1976 in favor of the liquid metal cooled fast reactor (LMFR)[9]; although the MSR technology was considered promising, LMFR was perceived to be more promising at the time. The MSBR design was a 2250 MWth reactor, optimized to breed ^{233}U from ^{232}Th in a single fluid system. Online pyrochemical reprocessing was planned to clean the fuel solvent from the neutron-absorbing fission products. Nevertheless, interruption of reactor operation was planned every 4 years to replace the graphite moderator, as experiments had revealed significant swelling of graphite due to radiation damage. Because of the (semi)continuous online clean up of the fuel, the addition of zirconium to the fuel was not necessary, and FLIBE could be used as carrier of the fertile (ThF_4) and fissile elements (UF_4). As secondary coolant, a NaF–$NaBF_4$ (8–92 mol%) mixture was foreseen because the retention of tritium, which is formed by neutron interaction with lithium and beryllium, is much better than FLIBE.

Also outside of the USA there was a strong interest in fast breeder MSR concepts. In UK,[11] Switzerland[12] and France[13] the focus was on chloride fueled systems. In all three cases a NaCl-UCl_3-$PuCl_3$ fuel salt was envisaged, with a relatively high content of heavy metals (> 30%). Because of the risk of formation of long-lived ^{36}Cl via neutron activation of natural ^{35}Cl, the chlorine in these systems was enriched in ^{37}Cl. The fuel inlet temperatures in these reactors were substantially lower than in fluoride concepts, and the Swiss SOFT concept had a 180 degrees increase from 743K to 923K. In the 1990s, the French REBUS concept was presented, strongly based on the earlier French work on chloride-fueled fast reactors.[14]

5.18.3 MSR Fuel Concepts

In the 1990s, there was a renewed interest in molten salt technology, which originated from programs that were looking into the possibilities of transmutation of actinides. When addressing transmutation of minor actinides, the absence of complicated fuel and fuel pin fabrication and the compatibility with pyrochemical processing in the molten salt fuel cycle were recognized as important advantages, in comparison with conventional pellet fuel types. Also, the interest in the use of thorium as a nuclear fuel kept up the interest in MSRs. Based on this and on the inherent safety features, the MSR has been selected as one of the Generation IV advanced reactor concepts selected to meet future energy needs.

The fuel in the MSR must fulfill several requirements with respect to its physicochemical properties (as will be discussed in Section 5.18.4). These requirements are very well met by the various systems containing alkali metal and alkali-earth fluorides and/or chlorides; hence the fluoride and chloride systems are nowadays the most recognized candidates for MSR fuels.

In the previous section, the MSBR has been mentioned as a graphite-moderated reactor that is based on the ^{7}LiF–BeF_2–$^{232}ThF_4$–UF_4 system.[3] $^{232}ThF_4$ is a fertile material that is used to produce fissile $^{233}UF_4$ by a neutron capture and two consecutive β-decays of ^{233}Th and ^{233}Pa. This fuel composition based on the FLIBE matrix still remains an ideal candidate when the MSR is designed as a thermal breeder reactor (moderated reactor). In this case, neutron economy is very critical and only isotopes with very low neutron

capture cross-section in the thermal spectrum can be part of the fuel matrix. Thus, ^{7}LiF and BeF_2 are the prime compounds for consideration. One of the current MSR concepts that uses fuel technology similar to that of the MSBR are Chinese Thorium Molten Salt Reactor (TMSR) concept, Indian Molten Salt Breeder Reactor (IMSBR) or the Japanese MSR FUJI concept.[15] The latter is a rather small graphite-moderated concept with an installed thermal capacity of 450 MW.

Many of current MSR designs, however, drift away from thermal graphite-moderated concepts, and favor non-moderated concepts that have a fast(er) neutron spectrum. Fuel selection for the non-moderated reactor concepts is more flexible, and elements other than ^{7}Li can be considered for the fuel solvent. One reason is that the neutron capture cross-section of the alkali halides and alkali-earth halides is generally lower in the "fast" spectrum than in the thermal spectrum; also, the neutron economy is not as sensitive in the "fast" spectrum as in the thermal one. Therefore Na, K or Rb cations can be considered as part of the fuel matrix. Moreover, increasing interest is to utilize chloride based salts which can be efficiently used in fast neutron spectrum systems.

The non-moderated reactors are attracting interest because they offer the possibility of transmuting the long-lived actinides produced mostly in light water reactors. The transmutation is most effective in the fast neutron spectrum; however, due to the presence of the fluorine atom in the fuel, partial moderation is maintained, and the neutron spectrum of the MSR is, rather, shifted to the epithermal range. Nevertheless, at this energy, all the minor actinides are fissionable, and the fission-to-capture ratio for these nuclides is still much higher than in the thermal spectrum.[16] Furthermore, the non-moderated reactor does not require graphite blocks (moderator in the thermal MSR) in the reactor core: they are very susceptible to radiation damage and must be periodically replaced.

Within the Generation IV platform, two main concepts for the non-moderated MSRs are studied nowadays. The first is an actinide burner design based on the Russian MOSART (Molten Salt Actinide Recycler and Transmuter) concept,[5] for which the ^{7}LiF–(NaF)–BeF_2–AnF_3 system is proposed as a fuel salt. The startup and feed material scenarios can include plutonium and minor actinides from pressurized water reactor (PWR) spent fuel. Depending upon the feed material, the fuel salt at equilibrium contains 0.7–1.3 mol% of actinide and lanthanide trifluorides. The second one is an innovative concept called MSFR (Molten Salt Fast Reactor), which has been developed within EU with leadership in France.[4,17–19] The fuel in this concept is based on the ^{7}LiF–$^{232}ThF_4$ matrix, with the addition of actinide fluorides as a fissile material. There are two initial fissile choices in the MSFR concept: (1) the ^{233}U-started MSFR and (2) the transuranic-started MSFR with a mix of 87.5% of Pu (^{238}Pu 2.7%, ^{239}Pu 45.9%, ^{240}Pu 21.5%, ^{241}Pu 10.7%, and ^{242}Pu 6.7%), 6.3% Np, 5.3% of Am, and 0.9% of Cm in the form of fluorides, corresponding to the transuranic element composition of a UO_2 fuel after one use in a PWR and 5 years of storage.[20]

A representative of MSR design based on chloride fuel salt is the REBUS-3700 concept. It is a fast breeder reactor proposed by Mourogov and Bokov[14] and it is based on a ^{238}U/^{239}Pu cycle, where ^{238}U serves as a fertile material bred to fissile ^{239}Pu by neutron capture and two consecutive β-decays of ^{239}U and ^{239}Np. Both uranium and plutonium are present in the form of trichlorides dissolved in a matrix of liquid NaCl.

In recent years, interest of utilizing this liquid fueled technology increased not only on a national level, but several start-up companies in Canada, the EU and the USA selected this technology with the goal of short(er) term deployment. This includes both large scale power plants (e.g., 1000 MWe) and small modular reactors (e.g., $<$300 MWe).

In the US, alternative concepts called the Advanced High-Temperature Reactor (AHTR) and the Fluoride cooled High temperature Reactor (FHR) are also being explored. The AHTR uses liquid salts (in FHR, it is specifically fluoride salt) as a coolant but used the graphite core structures and coated TRISO fuel particles of the Very High Temperature Reactor. The superior heat transport characteristics of salts compared to helium could enable power densities 4–6 times higher and power levels up to 4000 MWth with passive safety characteristics inherent in the design.[21]

The comprehensive list of MSR concepts studied nowadays as published in the GIF annual report[22] is summarized in **Fig. 1(b)**.

5.18.4 Properties of MSR Fuels and Coolants

Although the main focus of the past efforts done by ORNL, and without doubt the major historical achievement in the molten salt reactor history, was on fluoride salt systems, some concepts studied in that era by other countries, e.g., by France (REBUS-3700 concept[14]) considered chloride salts as fuel basis. Nowadays, and especially with the increased interest of many start-up companies in Europe and US in recent years, both fluoride and chloride salt media are considered. There are strong reasons for both halide families, but the right selection will depend on the exact molten salt reactor concept. Although more data exist on fluoride salts which is mainly due to the focus of ORNL in the past, it does not disqualify chlorides from consideration. There are gaps on physico-chemical properties data for both systems (bigger for chlorides), but some general statements can be drawn already when comparing both halide groups:

(1) Chloride salts melt at somewhat lower temperatures compared to fluorides, but metal halides of both groups melt well above room temperature. In general, lower melting points are better for the following two reasons: (1) less heat is needed to put the reactor into operation during start-up, and (2) the lower the melting point, the lower the operating temperature of the reactor, which can significantly mitigate potential corrosion of structural materials.

(2) Boiling points are generally lower for chlorides compared to fluorides, but both halides offer sufficient margin between melting points and boiling points.

Moreover, even the existing data for fluoride fuel salts that have been investigated in the past may need to be confirmed by novel measurements performed under quality assurance, as this may likely be a requirement imposed by licensing authorities.

In this section, the physicochemical properties of the primary MSR fuel and coolant choices summarized in **Table 2** are discussed, with the emphasis on the melting behavior, actinide solubility in the fuel matrix, density, viscosity, heat capacity, thermal conductivity, and vapor pressure. All these quantities are highly relevant for the reactor design calculations and a summary of these properties for typical coolant and fuel compositions is given in **Tables 3** and **4** respectively. Optimized phase diagrams of the relevant fluoride systems used as MSR fuels, coolants, or heat transfer salts are also shown in this section.

5.18.4.1 Structural Aspects of Molten Salts

Molten fluoride salts are essentially ionic liquids in which cations and anions form a loose network. Some cations occur in their simplest form, such as Li^+ and Na^+, but some form molecular species like BeF_2, which is a structural analog to SiO_2, known to be highly associated and forming a network structure that exhibits a glass transition characteristic. In a recent study by Salanne *et al.*,[23] a molecular dynamic study was performed on the LiF–BeF_2 system in order to understand the structure of the (Li,Be)F_{2-x} melt. **Fig. 2** shows the distribution of various species observed in the solution as a function of BeF_2 composition. At low concentrations of BeF_2 in LiF, the mixture behaves as a well-dissociated ionic melt consisting of Li^+, BeF_4^{2-}, and F^- species. As BeF_2 concentration increases, the

Table 2 The various applications of molten salts in nuclear reactor concepts

Reactor type	*Neutron spectrum*	*Application*	*Primary choice*	*Alternative(s)*
MSR breeder	Thermal	Fuel	^{7}LiF–BeF_2–AnF_4	
Fast	Fuel	^{7}LiF–AnF_4	^{7}LiF–CaF_2–AnF_4, NaCl–UCl_3–$PuCl_3$	
		Secondary coolant	NaF–$NaBF_4$	LiF–BeF_2, KF–KBF_4
MSR burner	Fast	Fuel	LiF–NaF–BeF_2–AnF_3	LiF–NaF–KF–AnF_3, LiF–NaF–RbF–AnF_3
AHTR[a]	Thermal	Primary coolant	^{7}LiF–BeF_2	
VHTR[b]	Thermal	Heat transfer[c]	LiF–NaF–KF	LiCl–KCl–$MgCl_2$
MS-FR[d]	Fast	Primary coolant	LiCl–NaCl–$MgCl_2$	
SFR[e]	Fast	Intermediate coolant[f]	$NaNO_3$–KNO_3	

[a]Advanced high-temperature reactor, graphite-moderated, thermal reactor.
[b]Very high-temperature reactor, graphite-moderated, gas cooled reactor.
[c]Heat transfer salt is a medium that will be used to deliver heat from the reactor to the hydrogen production plant.
[d]Molten salt cooled fast reactor, the solid fuel fast reactor with MS as a coolant.
[e]Sodium cooled fast reactor.
[f]To separate sodium and the steam circuits.

Table 3 Selected properties of the coolant salts

Property	*LiF–BeF_2 (0.66–0.34)*	*NaF–$NaBF_4$ (0.08–0.92)*	*LiF–NaF–KF (0.465–0.115–0.42)*
Melting point (K)	728	657 ± 1	727
ρ(kg m^{-3})	2146.3–0.4884T (K)	2446.3–0.711T (K)	2579.3–0.6240T (K)
η(mPa s)	1.81 exp (1912.2/T (K))	0.0877 exp (2240/T (K))	0.0248 exp (4477/T (K))
C_p(J K^{-1} g^{-1})	2.39	1.506	1.88
λ(W m^{-1} K^{-1})	1.1	$0.66–2.37 \times 10^{-4} T$ (K)	$0.36 + 5.6 \times 10^{-4} T$ (K)
$\log_{10}(p$(Pa))	11.914–13003/T (K)	11.638–6550.6/T (K)	10.748–10789/T (K)

Table 4 Selected properties of the fuel salts. Compositions in molar fractions

Property	*LiF–ThF_4 (0.78–0.22)*	*LiF–BeF_2–ThF_4 (0.717–0.16–0.123)*	*LiF–NaF–BeF_2–PuF_3 (0.203–0.571–0.212–0.013)*	*NaCl-UCl_3-$PuCl_3$ (0.55–0.294–0.156)*
Melting point (K)	841	771	775	873K
ρ(kg m^{-3})	5543.0–1.2500T (K)	4124.3–0.8690 T (K)	2759.9–0.5730 T (K)	3600[a]
η(mPa s)	0.365 exp (2735/T (K))	0.062exp(4636/T (K))	0.100 exp (3724/T (K))	–
C_p(J K^{-1} g^{-1})	1.0	1.55	2.15	0.908[a]
λ(W m^{-1} K^{-1})	$\sim$1.5[b]	1.5[b]	$0.402 + 0.5 \times 10^{-3}/T$ (K)	–
$\log_{10}(p$(Pa))	10.929–12280/T (K)	11.158–10, 790.5/T (K)	11.6509–12, 827/T (K)	–

[a]Value for T = 963K, taken from.[14]
[b]Value for T = 1023K.

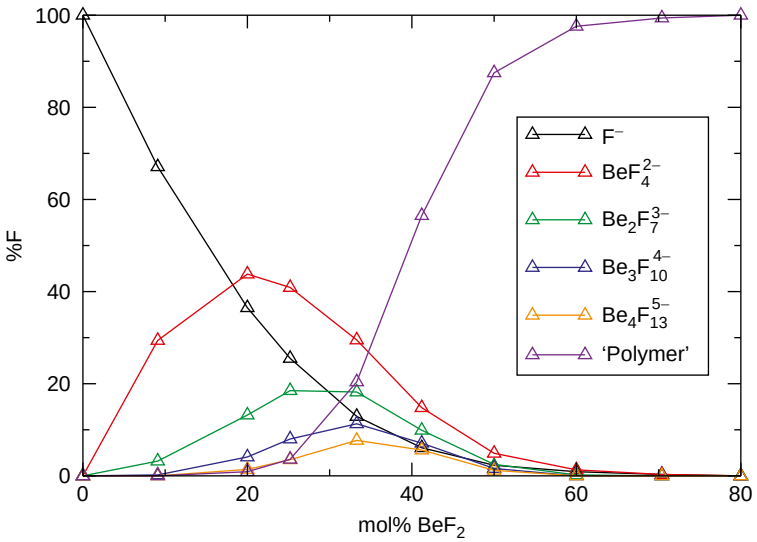

Fig. 2 Percentage of F-atoms involved in various species observed in the LiF–BeF_2 system as a function of composition; "polymer" means a cluster with a Be nuclearity > 4, whereas F^- implies that the ion is coordinated only to Li^+. Reproduced from Salanne, M., Simon, C., Turq, P., 2007. J. Phys. Chem. B 111, 4678–4684.

BeF_4^{2-} units start to bond together sharing a common F^- ion, first creating $Be_2F_7^{3-}$ species, followed by $Be_3F_{10}^{7-}$ species, and so forth, resulting in a polymer of several BeF_4^{2-} units. This polymerization is also a reason why the viscosity of pure BeF_2 is much higher compared to that of other fluorides discussed in this article. BeF_4^{2-} species were also experimentally observed by spectroscopic studies, as reported by Toth and Gilpatrick.[24] Lanthanide fluorides, ThF_4 or PuF_3 also form molecular species in their liquid form, but in comparison to BeF_2, they do not exhibit polymerization. Dracopolous *et al.*[25,26] investigated the structure of molten KF–YF_3 and KF–LnF_3 (Ln = La, Ce, Nd, Sm, Dy, Yb) systems using Raman spectroscopy and found that at $x(LnF_3) \leq 0.25$, LnF_6^{3-} are the predominant species surrounded by K^+ cations. At higher concentrations of LnF_3, the lanthanides are forced to share common fluorides and start to create loose structures of bridged octahedra. On the basis of these two studies, the authors concluded that lanthanide melts have similar structural behavior. In case of thorium, a tetravalent ion is the only known species in molten fluorides. As reported by Barton,[27] ThF_4 forms mainly anionic complexes of the general formula ThF_{4+m}^{m-}, and the existence of ThF_5^- is claimed.[28] In case of uranium, tri- or tetravalent ions are stable in the molten fluoride salt. It has been demonstrated[24] that UF_4 dissolves in the fluoride melts, forming complexes of coordination numbers 7 or 8. It has been shown that in fluoride-rich systems, the UF_8^{4-} species predominates, while with the reduction of fluoride ions, the UF_7^{3-} species is produced according to $UF_8^{4-} \rightleftharpoons UF_7^{3-} + F^-$. Furthermore, the same authors confirmed that approximately equal amounts of UF_8^{4-} and UF_7^{3-} occur in the LiF–BeF_2 melt of intermediate composition.

Also chloride melts are ionic liquids, in which molecular species form. The liquid of pure UCl_3 consists of networks of $[UCl_n]^{(n-3)-}$ clusters with n = 6,7,8, the corner-sharing, Cl-linked $[UCl_8]^{5-}$ being the dominant species, as derived from MD simulations.[29,30] This is one coordination number higher than the results of XAFS studies, which indicate an average coordination number of six, but in agreement with the interpretation of high-temperature X-ray diffraction measurements that also indicate $[UCl_8]^{5-}$. When diluting the UCl_3 with NaCl to about 40%, 6-coordination is dominant with 5 and 7 also present in substantial amounts. With increasing UCl_3 concentration, the 7- and 8-coordinated species are dominating for UCl_3 concentrations Above 25% polymeric $[U_nCl_m]$ species start to form.[31] Also UCl_4 forms $[UCl_n]$ clusters in NaCl, with the six-coordinated $[UCl_6]^{2-}$ species dominant at high UCl_4 concentrations, and $[UCl_6]^{2-}$ and $[UCl_7]^{3-}$ at low concentrations.

5.18.4.2 Phase Diagrams

5.18.4.2.1 LiF–BeF_2

The LiF–BeF_2 phase diagram has been assessed by van der Meer *et al.*[32] and more recently by Beneš and Konings,[33] the latter version being preferred as the authors considered not only the equilibrium points measured,[34–36] but also the mixing enthalpies of the $(Li,Be)F_x$ liquid solution measured by Holm and Kleppa.[37] The LiF–BeF_2 phase diagram is shown in **Fig. 3**; it is characterized by two eutectic invariant equilibria found at $T = 636$K and $x(BeF_2) = 0.517$, and $T = 729$K and $x(BeF_2) = 0.328$ in the calculation. Two intermediate phases, Li_2BeF_4 and $LiBeF_3$, are present in the system as well, the first melting congruently at $T = 729$K, whereas the latter decomposes below the solidus at $T = 557$K. A miscibility gap appears in the BeF_2-rich side, with the monotectic temperature found at $T = 772$K, while the critical temperature was found at $T_c = 812$K and $x(BeF_2) = 0.826$.

5.18.4.2.2 LiF–PuF_3

The thermodynamic assessment of the LiF–PuF_3 system was made in a study by van der Meer *et al.*[38] and later by Beneš and Konings,[39] using a different thermodynamic model based on the equilibrium data measured by Barton and Strehlow[40] and more

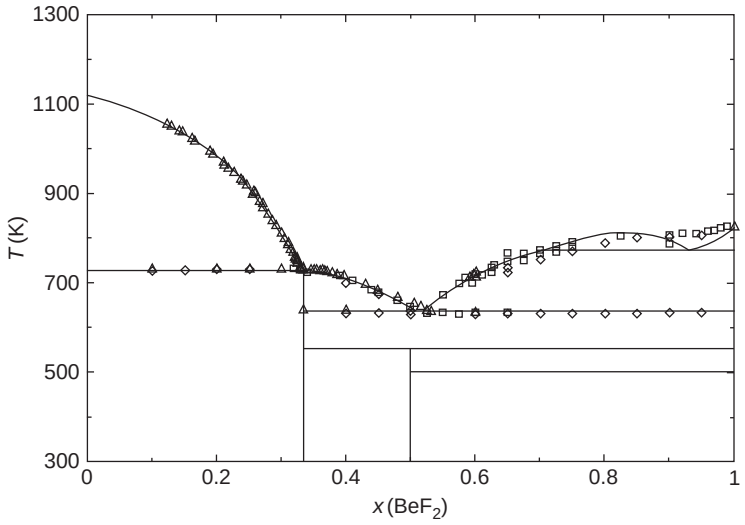

Fig. 3 Calculated LiF–BeF_2 phase diagram from Beneš and Konings: ◊ experimental data by Roy *et al.*; □ data by Thoma *et al.*; and △ data by Romberger *et al.* Reproduced from Beneš, O., Konings, R.J.M., 2009. J. Chem. Thermodyn. 41, 1086–1095. Roy, D.M., Roy, R., Osborn, E.F., 1954. J. Am Ceram. Soc. 37, 300. Thoma, R.E., Insley, H., Friedman, H.A., Hebert, G.M., 1968. J. Nucl. Mater. 27, 166. Romberger, K.A., Braunstein, J., Thoma, R.E., 1972. J. Phys. Chem. 76, 1154.

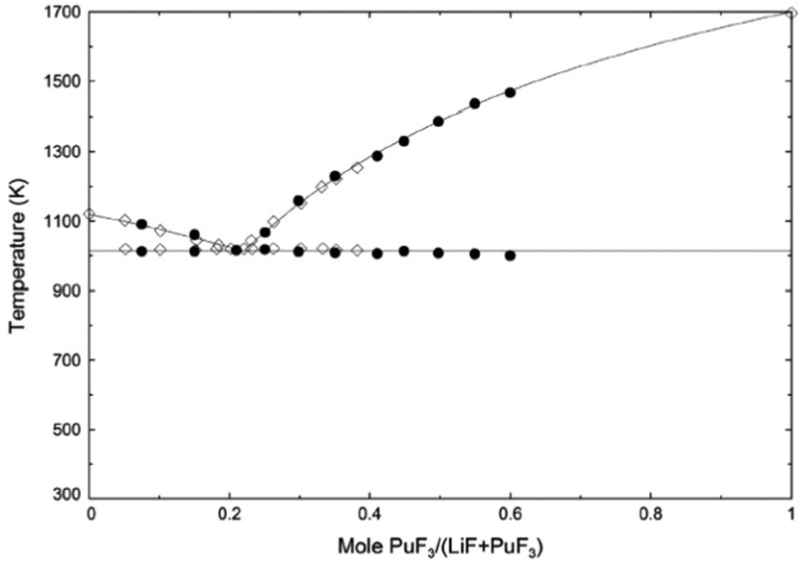

Fig. 4 The calculated LiF–PuF_3 phase diagram according to Beneš and Konings. (solid bullets) Data measured by Tosolin *et al.* (Open circles) Data obtained from Barton and Strehlow. Reproduced from Beneš, O., Konings, R.J.M., 2008. J. Nucl. Mater. 377 (3), 449–457. Barton, C.J., Strehlow, R.A., 1961. J. Inorg. Nucl. Chem. 18, 143–149. Tosolin, A., Souček, P., Beneš, O., *et al.*, 2018. J. Nucl. Mater. 503, 171–177.

recently by Tosolin *et al.*[41] who extended the data for compositions with richer PuF_3 concentrations. The calculated phase diagram based on the thermodynamic assessment of Beneš and Konings is shown in Fig. 4, indicating very good agreement with both experimental data.[40,41] The system is characterized by a single eutectic at $T=1018$K and $x\ (PuF_3) = 0.212$.

5.18.4.2.3 NaF–PuF_3

Similar to the LiF–PuF_3 system, the NaF–PuF_3 phase diagram has been thermodynamically assessed in two studies,[32,39] both based on the experimental data measured by Barton *et al.*[42] The phase diagram is shown in Fig. 5 and is characterized by one eutectic at $T=999$K and $x(PuF_3)=0.221$ and one peritectic at $T=1111$K and $x(PuF_3)=0.387$, where the $NaPuF_4$ intermediate compound decomposes.

5.18.4.2.4 BeF_2–PuF_3

To our best knowledge, there are no published experimental data on the BeF_2–PuF_3 system. Beneš and Konings[33] made a thermodynamic assessment of this system, assuming an ideal behavior of the liquid phase. The estimated BeF_2–PuF_3 phase diagram is shown in Fig. 6, characterized by a single eutectic point at $T=783$K and $x\ (PuF_3) = 0.031$.

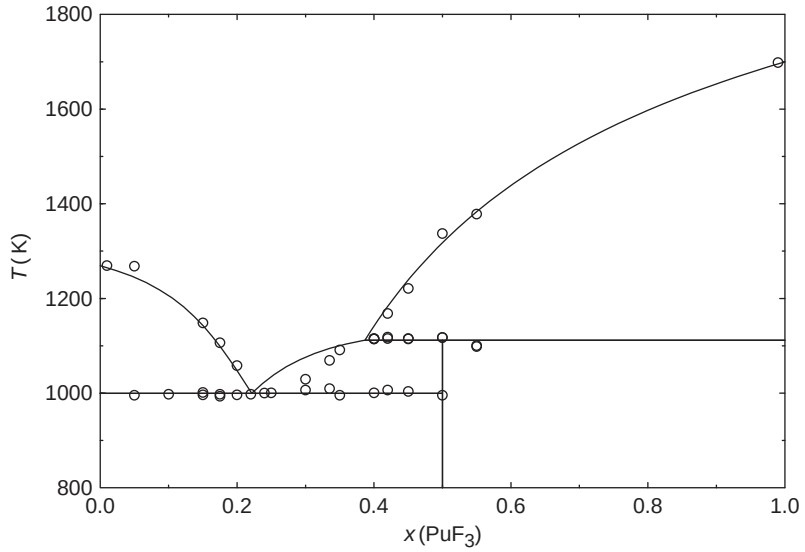

Fig. 5 The calculated NaF–PuF_3 phase diagram based on the thermodynamic data taken from Beneš and Konings: ○ experimental data measured by Barton *et al.* Reproduced from Beneš, O., Konings, R.J.M., 2008. J. Nucl. Mater. 377 (3), 449–457. Barton, C.J., Redman, J.D., Strehlow, R.A., 1961. J. Inorg. Nucl. Chem 20, 45–49.

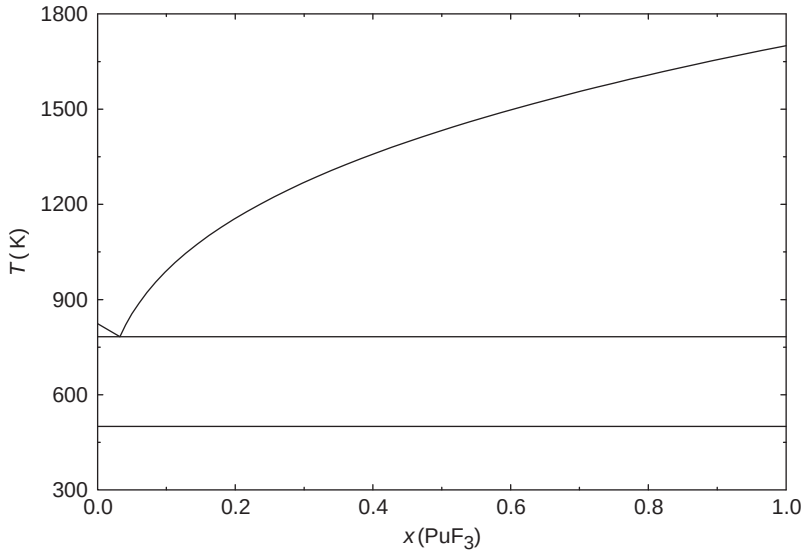

Fig. 6 The estimated BeF_2–PuF_3 phase diagram according to. Reproduced from Beneš, O., Konings, R.J.M., 2009. J. Chem. Thermodyn. 41, 1086–1095.

5.18.4.2.5 BeF_2–ThF_4

The BeF_2–ThF_4 system was assessed by van der Meer *et al.*[32] using the equilibrium data measured by Thoma *et al.*[43] The calculated phase diagram is shown in Fig. 7. It is a simple eutectic system with the eutectic at $T = 800$K and $x(ThF_4) = 0.019$.

5.18.4.2.6 LiF–AnF_4

The LiF–ThF_4 system is a reference salt for the MSFR concept. The equilibrium diagram of the LiF–ThF_4 system was reported by Thoma *et al.*[44] on the basis of thermal analysis and thermal quenching. Based on their data, the phase diagram was thermodynamically assessed by van der Meer *et al.*[32] and more recently by Beneš *et al.*[45] and Capelli *et al.*[46] The calculated phase diagram is shown in Fig. 8. The LiF–ThF_4 phase diagram consists of four mixed compounds: Li_3ThF_7, which melts congruently and $Li_7Th_6F_{31}$, $LiTh_2F_9$, and $LiTh_4F_{17}$, all melting peritectically. Two eutectic points were found at $X(ThF_4) = 0.224$ and $T = 841$K, and $X(ThF_4) = 0.283$ and $T = 838$K ThF_4, the first selected as a fuel solvent of the MSFR concept.[4]

In this notation, AnF_4 is represented mainly by ThF_4, which serves as a fertile material, and by UF_4, which is the fissile material, normally presented with a concentration of up to 4 mol%. As UF_4 and ThF_4 form close-to-ideal solid and liquid solutions, the melting

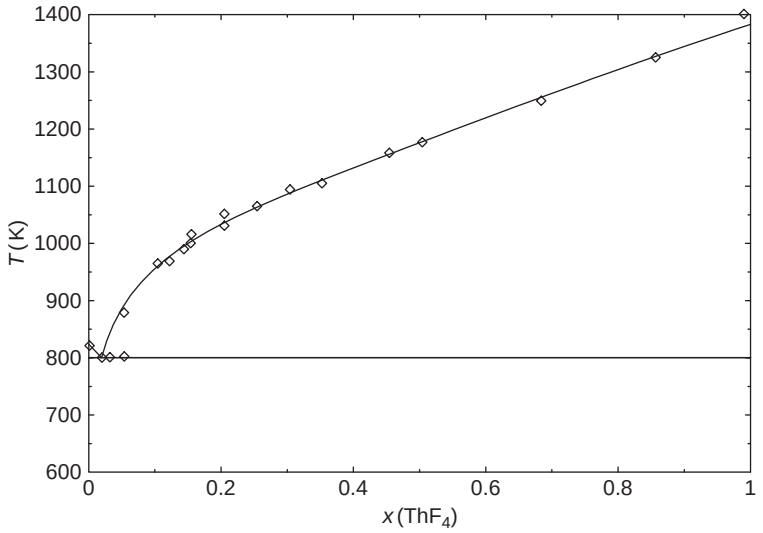

Fig. 7 The calculated BeF_2–ThF_4 phase diagram. Reproduced from van der Meer, J., Konings, R.J.M., Jacobs, M.H.G., Oonk, H.A.J., 2005. J. Nucl. Mater. 344, 94–99.

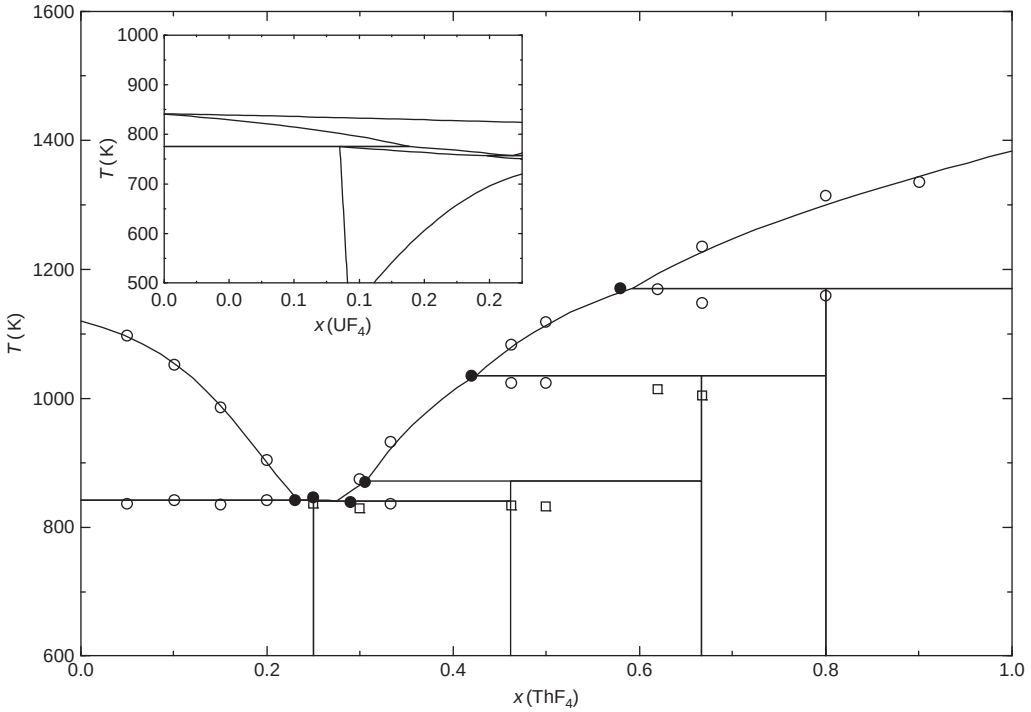

Fig. 8 The equilibrium diagram of the LiF–ThF_4 system assessed in Beneš *et al.*: ○ thermal analysis data obtained by Thoma *et al.*; □ supercooled data; • invariant equilibria as reported in Thoma *et al.* Inset: calculated ThF_4–UF_4 pseudobinary system with constant amount of LiF at 78 mol%. Reproduced from Beneš, O., Beilmann, M., Konings, R.J.M., 2010. J. Nucl. Mater. 405, 186–198. Thoma, R.E., Insley, H., Landau, B.S., Friedman, H.A., Grimes, W.R., 1959. J. Phys. Chem. 63, 1266.

point of the fuel is only slightly affected by the UF_4/ThF_4 substitution. The effect of UF_4 addition is demonstrated in the inset graph of Fig. 8, which shows the calculated liquidus line (the very upper line) of the ThF_4–UF_4 pseudobinary system with the amount of LiF constant at 78 mol%. The left axis of the graph corresponds to the proposed LiF–ThF_4 (78–22 mol%) fuel composition (eutectic$_1$ of the LiF–ThF_4 system) and the right axis corresponds to the LiF–UF_4 (78–22 mol%) composition; thus, in this case, all ThF_4 is substituted by UF_4. As can be seen from the figure, the liquidus line along this section is nearly constant, with a total drop of only 18K.

5.18.4.2.7 LiF–BeF_2–AnF_4

The LiF–BeF_2–ThF_4 system is the reference salt for a MSR designed as a thermal breeder. The equilibrium diagram of this system was measured by Thoma *et al.*[43] It contains lowest eutectic at 1.5 mol% ThF_4 and $T_{eut}=(629 \pm 3)$K; no ternary compounds were found. van der Meer *et al.*[47] calculated the ternary from the assessed binaries and found good agreement with the experimental diagram. More recently Capelli *et al.*[48] re-evaluated the phase diagram with novel experimental data on the LiF-ThF_4 binary system and found the lowest eutectic at T=632.2K and 1.8 mol% of ThF_4, in excellent agreement with the experimental data of Thoma *et al*. The calculated LiF–BeF_2–ThF_4 phase diagram of the latter study is shown in **Fig. 9**, as a projection of the liquidus surface.

In the reference MSBR concept, the proposed fuel composition in the LiF–BeF_2–AnF_4 system was 71.7–16.0–12.3, where the AnF_4 fraction was made up of 12.0 mol% ThF_4 and 0.3 mol% UF_4. In this section, AnF_4 is represented by pure ThF_4, which is possible for the chemical similarity between ThF_4 and UF_4. Assuming that the concentration of ThF_4 must be 12.3 mol%, it is possible, according to the thermodynamic data, to determine the lowest melting temperature of such a system and its exact composition. It has been found at $T=786$K and LiF–BeF_2–ThF_4 (67.1–20.6–12.3 mol%) (Composition 1), thus reasonably close to the data of the MSBR fuel ($T=771$K and LiF–BeF_2–AnF_4 (71.7–16.0–12.3 mol%) (Composition 2)). According to the modeled phase diagram presented in **Fig. 9**, the calculated liquidus temperature of the MSBR composition (Composition 2) is 795K.

As the melting temperatures of Compositions 1 and 2 are very close, we focus (see **Table 4**) the discussion only on the preferred composition of the MSBR concept (LiF–BeF_2–ThF_4 (71.7–16.0–12.3 mol%) (Composition 2)). This salt has also been more extensively studied, and thus more of its properties are known.

5.18.4.2.8 LiF–NaF–BeF_2–AnF_3

The LiF–NaF–BeF_2–PuF_3 system is a reference salt in the MOSART concept. The full thermodynamic description of this quaternary system has been assessed in a recent study by Beneš and Konings,[33] using the solubility data of PuF_3 measured by Barton,[49] Mailen *et al.*,[50] and Ignatiev *et al.*[51,52] for the optimization of the PuF_3-containing ternary subsystems. Based on this work[33] the optimized fuel composition is LiF–NaF–BeF_2–PuF_3 (20.3–57.2–21.2–1.3), which is exactly the point that corresponds to the lowest eutectic in the LiF–NaF–BeF_2–PuF_3 system, with a fixed concentration of PuF_3 at 1.3 mol% as an equilibrium concentration of AnF_3 after 10 years of operation of the MOSART reactor.[53] Note here that, in order to simplify the study, all actinides were represented by

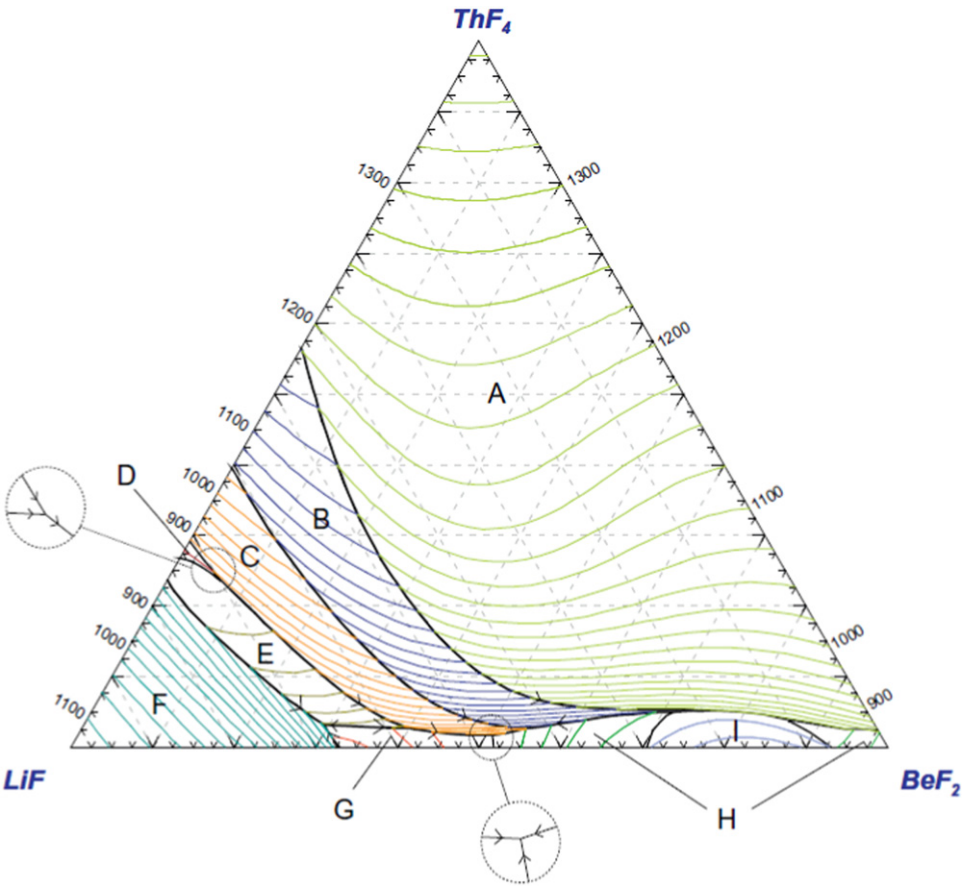

Fig. 9 The liquidus projection of the assessed LiF–BeF_2–ThF_4 system. Primary crystallization fields: A–ThF_4; B–$LiTh_4F_{17}$; C–$LiTh_2F_9$; D–$LiThF_5$; E–Li_3ThF_7s:s:; F–LiF; G–Li_2BeF_4; H–β-BeF_2; I–liquid (miscibility gap). *Source*: Capelli, E., Beneš, O., Konings, R. J. M., 2015. Trans. Am. Nucl. Soc. 112, 395–396.

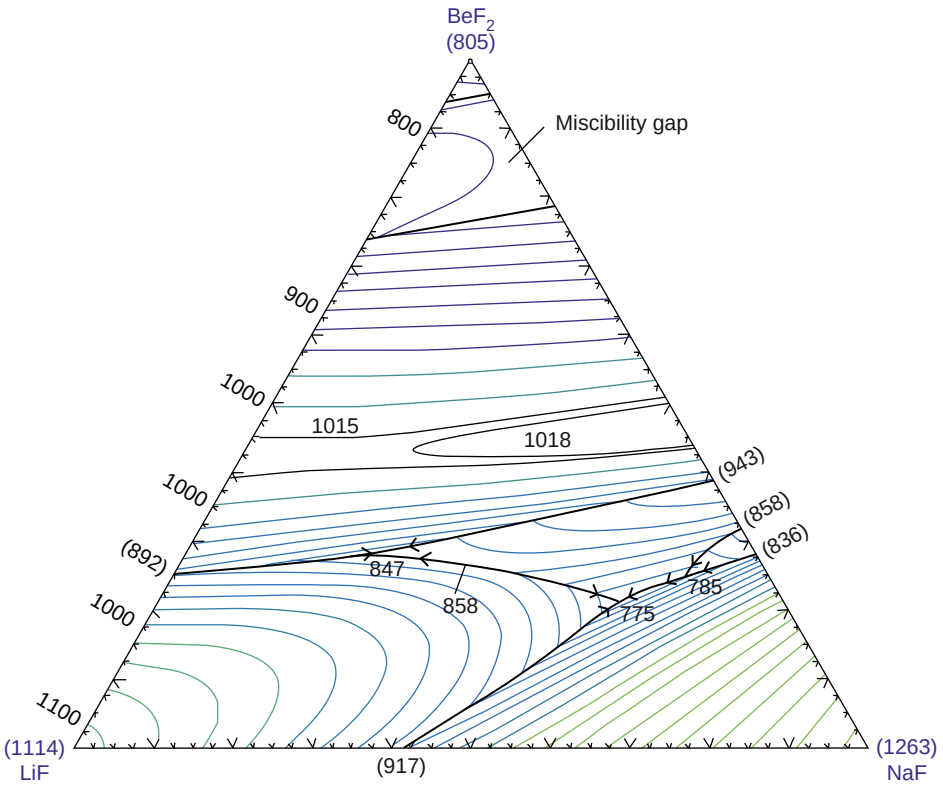

Fig. 10 Calculated pseudoternary phase diagrams of the LiF–NaF–BeF_2 system with constant amount of PuF_3 = 1.3 mol%. Reproduced from Beneš, O., Konings, R.J.M., 2009. J. Fluor. Chem. 130, 22–29.

plutonium. This was possible as plutonium is the major constituent of all actinides considered in the MOSART fuel. A pseudo-ternary phase diagram of the LiF–NaF–BeF_2–(PuF_3 = 1.3 mol%) system is shown in **Fig. 10**. The melting temperature of the lowest eutectic composition is calculated at 775K, which is much lower than the designed inlet temperature of the MOSART concept[6] and therefore acceptable for reactor purposes.

The optimized fuel composition as found in Beneš and Konings[33] varies slightly from that of the MOSART concept (LiF–NaF–BeF_2–PuF_3 (14.8–57.4–26.5–1.3)). Because the authors of the MOSART concept did not have a full thermodynamic description of the whole LiF–NaF–BeF_2–PuF_3 system, they took the eutectic of the LiF–NaF–BeF_2 system with the lowest BeF_2 content, as reported in Thoma,[54] and directly dissolved 1.3 mol% of AnF_3 in it. Hence, they did not consider the shift of the eutectic composition while adding AnF_3, which was demonstrated in Beneš and Konings.[33]

5.18.4.2.9 NaCl–UCl_3

The NaCl–UCl_3 system was thermodynamically assessed by Beneš and Konings[55] based on the experimental data by Taube[56] and the resulting phase diagram is shown in **Fig. 11**. It is a simple eutectic system with T = 793K and x(UCl_3) = 0.329. This is in excellent agreement with measurements of Taube who derived the same temperature and x(UCl_3) = 0.320. These results were recently confirmed by a study by Sooby *et al.*[57]

5.18.4.2.10 NaCl–$PuCl_3$

NaCl-$PuCl_3$ is another simple eutectic system and the phase diagram has been measured by Bjorklund *et al.*[58] They reported a eutectic point at T = 726K and x ($PuCl_3$) = 0.360. This is in agreement with the thermodynamic assessment performed by Beneš and Konings[55] who found eutectic at T = 725K and x ($PuCl_3$) = 0.383. The calculated NaCl–$PuCl_3$ phase diagram is shown in **Fig. 12**.

5.18.4.2.11 NaCl–UCl_3–$PuCl_3$

The liquidus projection of the NaCl-UCl_3-$PuCl_3$ phase diagram has been assessed by Beneš and Konings[55] and is shown in **Fig. 13**. It is simple ternary system with no ternary invariant equilibria. The melting minimum is found close to the NaCl-$PuCl_3$ binary eutectic, at T = 722K and x (NaCl) = 0.594, x (UCl_3) = 0.045 and x ($PuCl_3$) = 0.360.

5.18.4.2.12 NaF–$NaBF_4$

The equilibrium diagram of the NaF–$NaBF_4$ system was studied by Selivanov and Stender,[59] and Barton *et al.*[60] Both studies indicate that it is a simple eutectic system, but the eutectic temperatures and compositions differ considerably. In view of their

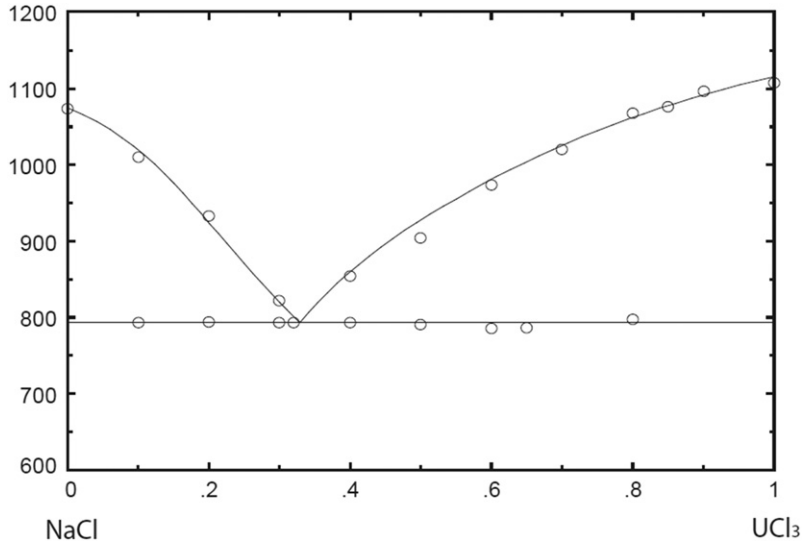

Fig. 11 The NaCl–UCl_3 system calculated according to the thermodynamic assessment by Beneš and Konings, ○ experimental data by Taube. *Source*: Beneš, O., Konings, R.J.M., 2008. J. Nucl. Mater. 375, 202–208. Taube, M., 1978. Fast Reactors Using Molten Chloride Slats as Fuel. Würenlingen: Swiss Federal Institute for Reactor Research.

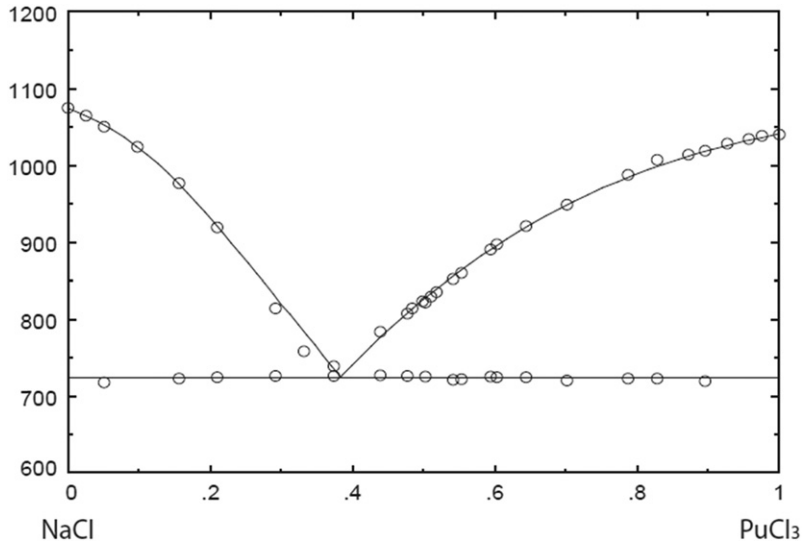

Fig. 12 The NaCl–$PuCl_3$ system calculated according to the thermodynamic assessment by Beneš and Konings, ○ experimental data by Bjorklund *et al.* *Source*: Beneš, O., Konings, R.J.M., 2008. J. Nucl. Mater. 375, 202–208. Taube, M., 1978. Fast Reactors Using Molten Chloride Slats as Fuel. Würenlingen: Swiss Federal Institute for Reactor Research. Bjorklund, C.W., Reavis, J.G., Leary, J.A., Walsh, K.A., 1959. J. Phys. Chem. 63, 1774–1777.

more careful sample preparation, the results of Barton *et al.* are preferred, and this diagram is shown in **Fig. 14**. They found $x_{eut}=(92 \pm 1)$ mol% $NaBF_4$ with $T_{eut}=(657 \pm 1)$K.

5.18.4.2.13 LiF–NaF–KF

A eutectic mixture of LiF, NaF, and KF is one of the possible candidates as an intermediate heat transfer salt used to deliver the heat from the high-temperature reactor (advanced high-temperature reactor (AHTR) or very high-temperature reactor (VHTR)) to, for example, a hydrogen production plant. Alternatively, the LiF–NaF–KF mixture can be considered as a solvent for actinide trifluorides in the molten salt actinide burner concept.

The LiF–NaF–KF phase diagram was measured by Bergmann and Dergunov,[61] who found the ternary eutectic with the lowest melting point at $T=727$K and LiF–NaF–KF (46.5–11.5–42.0 mol%). Thermodynamic assessment of this system was done in several

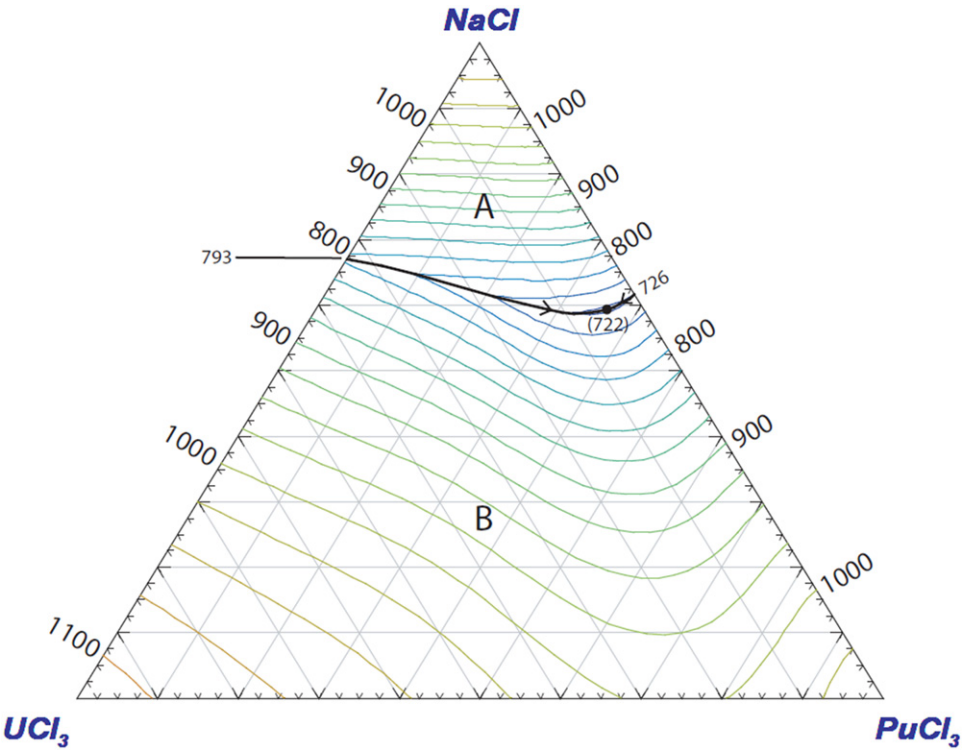

Fig. 13 Calculated NaCl–UCl_3–$PuCl_3$ phase diagram according to thermodynamic assessment of Beneš and Konings. *Source*: Beneš, O., Konings, R.J.M., 2008. J. Nucl. Mater. 375, 202–208.

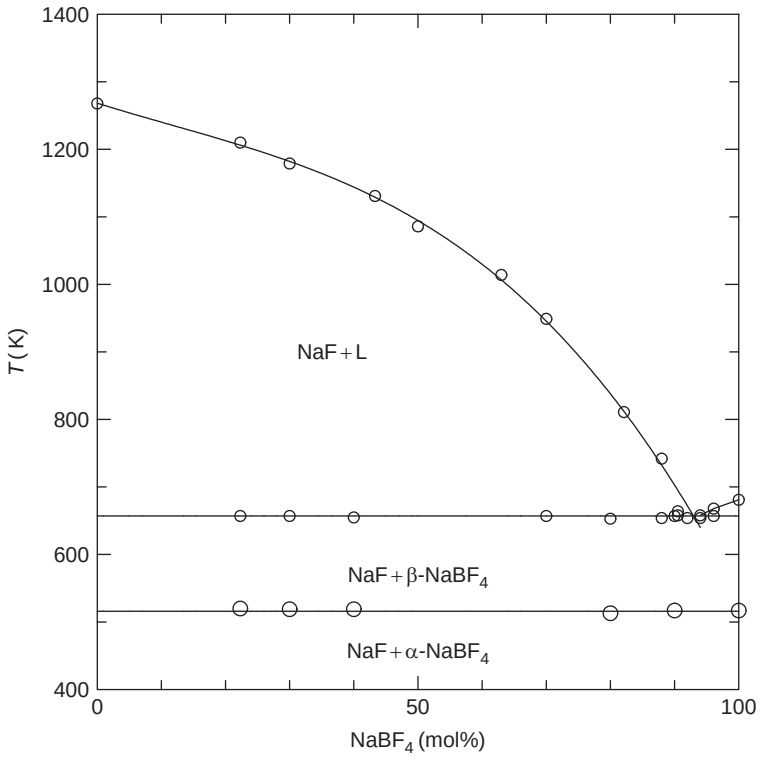

Fig. 14 The equilibrium diagram of the NaF–$NaBF_4$ system. Reproduced from Beneš, O., Konings, R.J.M., 2009. J. Fluor. Chem. 130, 22–29.

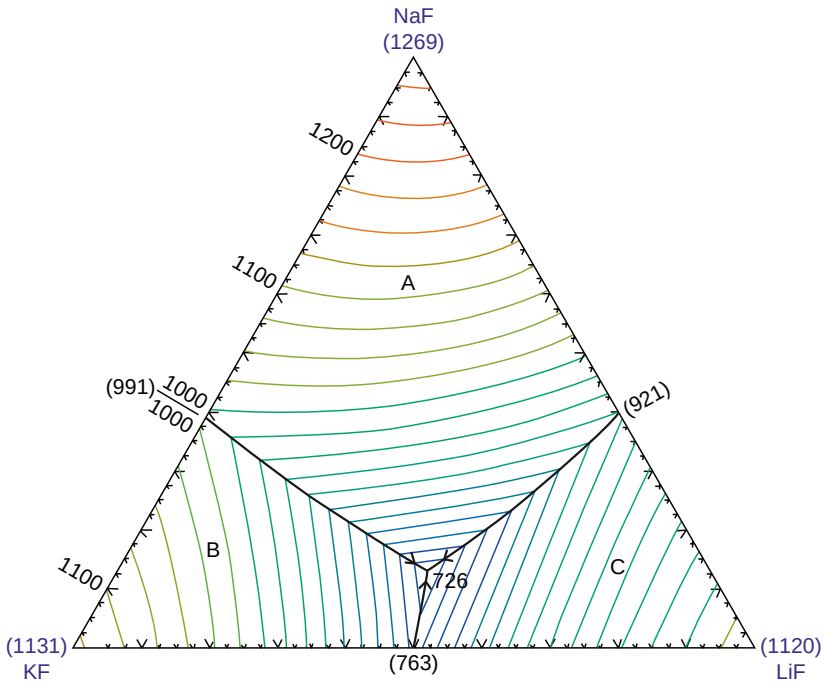

Fig. 15 Calculated liquid surface of the LiF–NaF–KF phase diagram. Isotherms are labeled in K with interval of 25K. Primary phase fields: (A) (Li,Na,K)F; (B) (Na,K)F; (C) (Li,Na)F. Reproduced from Beneš, O., Konings, R.J.M., 2009. J. Fluor. Chem. 130, 22–29. Beneš, O., Konings, R.J.M., 2008. Comput. Coupl. Phase Diagr. Thermochem. 32, 121–128.

studies,[62–64] all of which were in close agreement. **Fig. 15** shows the LiF–NaF–KF phase diagram calculated using the data from the study by Beneš and Konings,[64] who found the ternary eutectic at $T=726$K and LiF–NaF–KF (45.3–13.2–41.5 mol%).

5.18.4.3 Solubility of Actinides

5.18.4.3.1 ThF_4 in molten LiF

The solubility of ThF_4 in a matrix of LiF can be deduced from the binary phase diagram in **Fig. 8**. For example, the solubility of ThF_4 in a melt of LiF for $T=903$K (inlet temperature of the MSFR concept that is based on this fuel system) is between 20.0 and 32.3 mol%. Compositions in this range are, thus, of interest as fuel for the MSFR. In practice, the LiF–ThF_4 (78–22 mol%) composition is the prime choice.

5.18.4.3.2 ThF_4 in molten LiF–BeF_2

The solubility of ThF_4 in the LiF–BeF_2 matrix has been calculated for $T=839$K (inlet temperature of MSBR), keeping a constant ratio of LiF/BeF_2 = 0.818/0.182. This ratio corresponds to the fuel composition proposed in MSBR. **Fig. 16** shows the ternary phase diagram of the LiF–BeF_2–ThF_4 system at $T=839$K. The straight bold line represents the LiF/BeF_2 ratio at 0.818/0.182 within the whole field of the diagram, while the ThF_4 concentration varies from 0 to 100 mol% as it moves from point "C" towards "D". The solubility of ThF_4 in the LiF–BeF_2 matrix thus derived is between 9.2 and 20.8 mol%. The interval of the solubility is represented by the "A" and "B" signs, respectively, which correspond to the intersection of the "CD" line with the surface of the liquid field.

5.18.4.3.3 UF_4 in molten LiF–ThF_4

To our best knowledge, there are no experimental data of the UF_4 solubility in the LiF–ThF_4 binary matrix. However, based on the thermodynamic assessment of the LiF–NaF–ThF_4–UF_4 system,[45] the solubility of UF_4 in the LiF–ThF_4 (78 − 22) composition (primary fuel choice of the MSFR concept) has been calculated for a temperature range of 840–880K giving:

$$\log_{10} Q(\text{mol}\%) = 42.7475 - 0.1052T(\text{K}) + 6.6086 \times 10^{-5}T^2(\text{K}) \quad (1)$$

5.18.4.3.4 PuF_3 in molten LiF–BeF_2

The solubility of PuF_3 in the LiF–BeF_2 binary melt has been measured by Barton[27] and Mailen *et al.*[50] Barton measured the PuF_3 solubility in LiF–BeF_2 (71.3–28.7) and LiF–BeF_2 (63 − 37) compositions for the temperature range of 736–927K, whereas Mailen *et al.* measured the PuF_3 solubility in LiF–BeF_2 (67 − 33) composition for the temperature range of 59–657K. Furthermore, Barton measured the PuF_3 solubility at $T=838$K in the LiF–BeF_2 matrix as a function of composition from x(LiF) = 0.52–0.72. Beneš and Konings[33] thermodynamically evaluated the LiF–NaF–BeF_2–PuF_3 system and found very good agreement with all experimentally

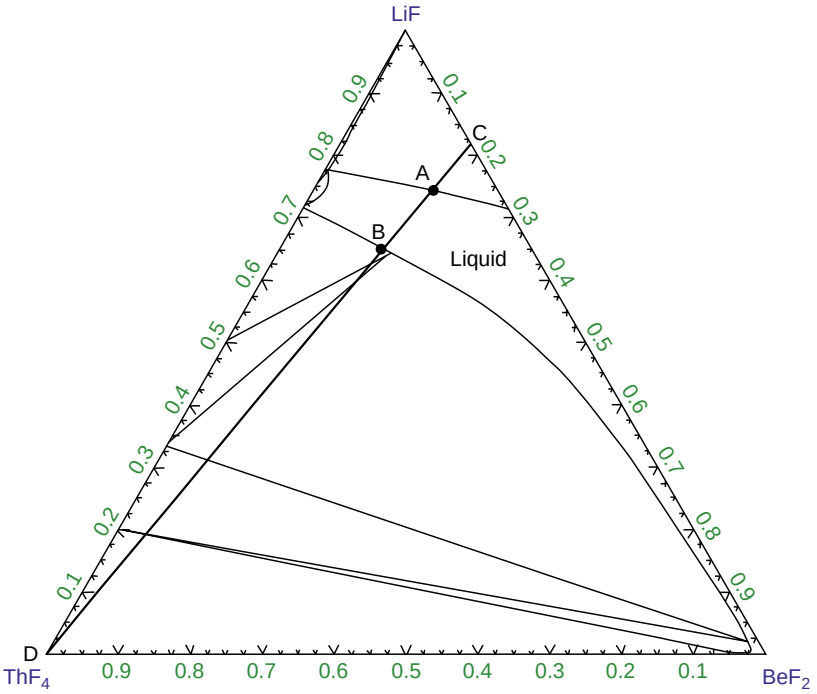

Fig. 16 Isothermal plot of the LiF–BeF_2–ThF_4 phase diagram at $T=839$K. Reproduced from Beneš, O., Konings, R.J.M., 2009. J. Fluor. Chem. 130, 22–29.

determined solubility data by Barton and Mailen *et al.* On the basis of their assessment, the PuF_3 solubility in the LiF–BeF_2 (67 – 33) composition has been calculated for the temperature range of 780–930K, giving:

$$\log_{10} Q(\text{mol}\%) = -4.0975 + 4.32 \times 10^{-3} T(\text{K}) \tag{2}$$

5.18.4.3.5 PuF_3 in molten LiF–NaF–BeF_2

According to the thermodynamic model of the LiF–NaF–BeF_2–PuF_3 system published in Beneš and Konings,[33] the solubility of PuF_3 in the recommended fuel matrix composition (LiF–NaF–BeF_2 (20.6–57.9–21.5)) was calculated for the temperature range of 823–973K and fitted with the polynomial equation below:

$$\log_{10} Q(\text{mol}\%) = -5.3526 + 9.7386 \times 10^{-3} T(\text{K}) - 3.4105 \times 10^{-6} T^2(\text{K}) \tag{3}$$

Based on this equation, the total PuF_3 solubility in the LiF–NaF–BeF_2 (20.6–57.9–21.5) melt at the inlet temperature of the MOSART reactor concept ($T=873$K) is 3.55 mol%. This value is slightly higher than the measured value in the MOSART matrix composition (LiF–NaF–BeF_2 (15–58–27)), which was determined to be 3.08 mol%.[66] Higher solubility was achieved in the former case because of the lower content of BeF_2, which is the main fuel component responsible for low AnF_3 solubility, as discussed in Beneš and Konings.[33]

5.18.4.3.6 PuF_3 in molten LiF–BeF_2–ThF_4

The solubility of PuF_3 in various compositions of LiF–ThF_4 and LiF–BeF_2–ThF_4 melts were measured by Sood *et al.*,[67] between 783 and 1060K. Results of their measurements are reported in **Table 5**, showing the derived coefficients for the general equation:

$$\log_{10} Q(\text{mol}\%) = \text{A} + B/T(\text{K}) \tag{4}$$

5.18.4.3.7 UCl_3 in molten NaCl

The solubility of UCl_3 in the NaCl melt can be derived from the NaCl-UCl_3 binary phase diagram, shown in **Fig. 11**, following the liquidus line with respect to the composition and temperature. According to the phase diagram the solubility range of UCl_3 in the matrix of NaCl at 843K, a temperature 50K above the lowest eutectic point ($T_{eut.}=793$K), is 27.7–38.0 mol%.

5.18.4.3.8 $PuCl_3$ in molten NaCl

The solubility of $PuCl_3$ in the NaCl melt can be derived from the NaCl-$PuCl_3$ binary phase diagram, shown in **Fig. 12**, following the liquidus line as described in the previous case. According to the phase diagram the solubility range of $PuCl_3$ in the matrix of NaCl at 775K, a temperature 50K above the lowest eutectic point ($T_{eut.}=725$K), is 34.0–43.9 mol%.

Table 5 Solubility of PuF_3 in the LiF–BeF_2–ThF_4 melts measured by Sood *et al.*

Salt composition (mol%)			*Temperature range (K)*	*A*	$-B \times 10^{-3}$
LiF	BeF_2	ThF_4			
74.0	22.1	3.9	851–1021	3.55 ± 0.14	2.97 ± 0.14
76.9	17.1	6.0	878–973	3.49 ± 0.23	2.82 ± 0.21
75.3	16.7	8.0	812–1029	3.80 ± 0.05	3.13 ± 0.04
68.2	20.5	11.3	821–1049	2.98 ± 0.05	2.52 ± 0.06
71.6	16.2	12.2	796–1031	2.95 ± 0.07	2.46 ± 0.07
71.3	15.5	13.2	783–1060	2.62 ± 0.07	2.15 ± 0.06
70.0	14.0	16.0	802–949	2.56 ± 0.11	2.06 ± 0.10
75.0	5.0	20.0	826–1038	2.57 ± 0.14	1.84 ± 0.13
80.0	0.0	20.0	926–1054	2.62 ± 0.19	1.78 ± 0.19
75.0	0.0	25.0	882–1038	2.58 ± 0.05	1.76 ± 0.05
70.0	0.0	30.0	873–1018	2.84 ± 0.07	1.99 ± 0.07
65.0	0.0	35.0	935–1026	3.01 ± 0.08	2.20 ± 0.08

Note: Sood, D.D., Iyer, P.N., Prasad, R., *et al.*, 1975. Nucl. Technol. 27, 411–416.

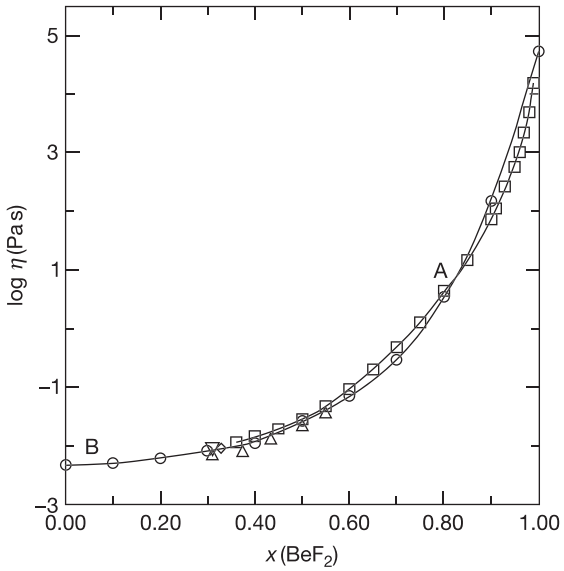

Fig. 17 The viscosity of liquid LiF–BeF_2 at 873K: ▽ Cohen and Jones; △ Blanke *et al.*; □ (curve A), Cantor *et al.*; ○ (curve B), Desyatnik *et al.*; ◊ Abe *et al.* Reproduced from Beneš, O., Konings, R.J.M., 2009. J. Fluor. Chem. 130, 22–29. Cohen, S.I., Jones, T.N., 1957. Technical Report ORNL-2278. Blanke, B.C., Bousquet, E.N., Curtis, M.L., Murphy, E.L., 1956. Technical Report USAEC MLM-1086. Cantor, S., Ward, W.T., Moynihan, C.T., 1969. J. Chem. Phys. 50, 2874. Desyatnik, V.N., Nechayev, A.I., Chervinskii, Y.F., 1981. Zh. Prikl. Khim. 54, 2310–2312. Abe, Y., Kosugiyama, O., Nagashima, A., 1981. J. Nucl. Mater. 99, 173–183.

5.18.4.4 Density and Viscosity

5.18.4.4.1 LiF–BeF_2

The density of liquid LiF–BeF_2 has been measured by Blanke *et al.*[68] from 0 to 55 mol% BeF_2, by Cantor *et al.*[69] for 50.2, 74.9, and 89.2 mol% BeF_2, and by Cantor[70] for the 34 mol% BeF_2 composition. As discussed by van der Meer *et al.*,[38] the molar volumes derived from the measured density data indicate ideal behavior, suggesting that the density can be interpolated from the molar volume data for the pure components. However, the density and molar volume of liquid BeF_2 are known only at a single temperature ($T = 1073$K), and not at all as a function of temperature. Therefore, we have selected the results of the 66–34 mol% composition from Cantor[70]:

$$\rho\left(\mathrm{kg\ m^{-3}}\right) = 2146.3 - 0.4884T(\mathrm{K}) \tag{5}$$

The viscosity of liquid LiF–BeF_2 has been measured by Cohen and Jones[71] and Abe *et al.*[72] for the compositions 31 and 32.8 mol% BeF_2, respectively, as well as by Blanke *et al.*,[68] Cantor *et al.*,[69] and Desyatnik *et al.*[73] for a wide(r) range of compositions and temperatures. The agreement between the studies is excellent, as shown in Fig. 17 in an isothermal section at 873K. From the results, we interpolate for the 66–34 mol% composition:

$$\eta(\mathrm{mPa\ s}) = 0.116 \exp\left(3755/T(\mathrm{K})\right) \tag{6}$$

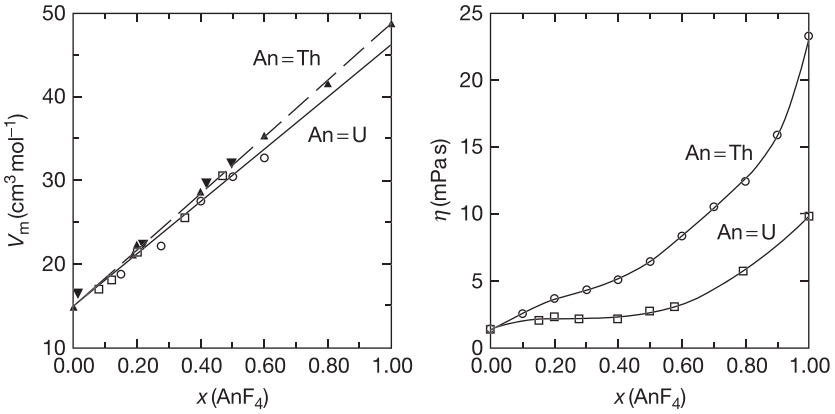

Fig. 18 The molar volume (left) and viscosity (right) of liquid LiF–ThF_4 and LiF–UF_4 at 1273K. Right figure: ○ data by Chervinskij *et al.*; □ data by Desyatnik *et al.*; Left figure: ▲ data by Hill *et al.*; ▼ data by Porter and Meaker; □ data by Blanke *et al.*; ○ data by Porter and Meaker. Reproduced from Beneš, O., Konings, R.J.M., 2009. J. Fluor. Chem. 130, 22–29. Chervinskii, Y.F., Desyatnik, V.N., Nechaev, A.I., 1982. Zh. Fiz. Khim. 56, 1946–1949. Desyatnik, V.N., Nechaev, A.I., Chervinskii, Y.F., 1979. Russ. J. Phys. Chem. 53, 986–988. Hill, D.G., Cantor, S., Ward, W.T., 1967. J. Inorg. Nucl. Chem. 29, 241–243. Porter, B., Meaker, R.E., 1966. Technical Report BMI RI-6836. Blanke, B.C., Bousquet, E.N., Curtis, M.L., Murphy, E.L., 1956. Technical Report USAEC MLM-1086.

5.18.4.4.2 LiF–AnF_4

The density of LiF–ThF_4 mixtures was measured by Porter and Meaker[74] and Hill *et al.*[75] The data are in good agreement and clearly indicate a linear dependence of the molar volume on composition as shown in **Fig. 18**, confirming ideal behavior. The density of the 78–22 composition as measured by Porter and Meaker, is given by:

$$\rho\left(\text{kg m}^{-3}\right) = 5543 - 1.25T(\text{K}) \tag{7}$$

The density of liquid LiF–UF_4 mixtures were measured by Blanke *et al.*[68] and Porter and Meaker.[74] The results are in excellent agreement, as shown in **Fig. 18**. The results indicate a linear dependence of the molar volume on composition, confirming ideal behavior.

The viscosity of LiF–ThF_4 mixtures was measured by Chervinskij *et al.*[76] from 0 to 100 mol% ThF_4. The results reveal a strong deviation from ideal behavior around the eutectic composition. An isothermal section in **Fig. 15** shows a steady increase from LiF to ThF_4. The viscosity of the 78–22 composition interpolated from the results is given by:

$$\eta(\text{mPa s}) = 0.365 \exp\left(2735/T(\text{K})\right) \tag{8}$$

The viscosity of the LiF–UF_4 system measured by the same group[77] shows a less strong increase with the AnF_4 content compared to ThF_4 (**Fig. 18**). As a result, the above equation probably overestimates the viscosity slightly in the case of part replacement of ThF_4 by UF_4.

5.18.4.4.3 LiF–BeF_2–ThF_4

The densities of the three compositions of the LiF–BeF_2–ThF_4 system, with almost constant LiF concentration, were measured by Cantor.[70] Unfortunately, the density of the LiF–BeF_2–ThF_4 (71.7–16.0–12.3) composition has not been measured; however, a very close composition (LiF–BeF_2–ThF_4 (70.06–17.96–11.98)) has been determined and the corresponding density function is given below:

$$\rho\left(\text{kg m}^{-3}\right) = 4043.9 - 0.8064T(\text{K}) \tag{9}$$

It has been shown by van der Meer and Konings[78] that the molar volumes and thus the densities of all three LiF–BeF_2–ThF_4 compositions measured in Cantor[70] behave almost ideally. Based on this triplet of data and with the assumption of the ideality, it is possible to estimate the density function of temperature of pure BeF_2, which has not been measured yet. The density of liquid BeF_2 was measured by Mackenzie,[79] but only at 1073K, obtaining the value of 1947 $\pm$ 10 kg m^{-3}. Cantor *et al.*[69] also measured the density, but, due to the experimental difficulties, they derived only an approximate value: 1960 kg m^{-3} at 1123K. The value of MacKenzie is recommended and taken as a constraint in our estimation. The obtained density for liquid BeF_2 as a function of temperature is shown below:

$$\rho\left(\text{kg m}^{-3}\right) = 3190.5 - 1.1589T(\text{K}) \tag{10}$$

Using Eq. (10) together with the selected data for the LiF and ThF_4 densities taken from van der Meer and Konings,[78] we have calculated the expected density function of temperature for the LiF–BeF_2–ThF_4 (71.7–16.0–12.3 mol%) composition (MSBR). The obtained equation is given below:

$$\rho\left(\text{kg m}^{-3}\right) = 4124.3 - 0.8690T(\text{K}) \tag{11}$$

The results from Eqs. (9) and (11) agree very well. As the former equation is based on the experimental results whereas the latter is an estimate, and both equations refer to very similar compositions, the extrapolation of the density in the LiF–BeF_2–ThF_4 system can be justified on the basis of ideal behavior. Based on Eq. (11), the density of the salt mixture at $T=973$K is 3279 kg m^{-3}, for the LiF–BeF_2–ThF_4–UF_4 (71.0–16.0–12.0–1.0 mol%) composition, while the reported density at the same temperature taken from the study by Briant and Weinberg[80] is 3250 kg m^{-3}: values that are in close agreement.

The viscosity of liquid LiF–BeF_2–ThF_4 of two compositions was measured by Cantor.[70] The viscosity of the quaternary LiF–BeF_2–ThF_4–UF_4 (71–16–12–1) composition, which is nearly identical to our reference selection (LiF–BeF_2–ThF_4 (71.7–16–12.3)), has been reported in Powers *et al.*[81] for the temperature range of 873–1073K, giving:

$$\eta(\text{mPa s}) = 0.062 \exp(4636/T(\text{K})) \tag{12}$$

5.18.4.4.4 LiF–NaF–BeF_2–AnF_4

Densities of several LiF–NaF–BeF_2 mixtures have been measured in various studies,[66,81] but the exact compositions are different from that of our recommended fuel choice from **Table 4**. However, in a recent study by Khokhlov *et al.*[82] the density of a very similar ternary mixture (LiF–NaF–BeF_2 (22–56.7–21.3 mol%)) was estimated, using an additive law of molar volumes according to the equation $V=\sum N_i V_i$, where V_i is a molar volume of LiF and NaF end members, and LiF–BeF_2 and NaF–BeF_2 mixtures, whose compositions are shown in square brackets in the following notations: [0.508LiF–0492BeF_2]–0.567NaF; [0.727NaF–0.273BeF_2]–0.22LiF. The density of the ternary mixture was taken as a mean value from these two notations, and the temperature function thus derived is shown below:

$$\rho(\text{g m}^{-3}) = 2.5777 - 5.38 \times 10^{-4} T(\text{K}) \tag{13}$$

Densities of binary LiF–BeF_2 and NaF–BeF_2 mixtures were measured as a function of temperature and composition and taken from the work of Janz[83] as reported in Khokhlov *et al.*[82] Khokhlov *et al.* also made calculations for the same compositions as measured by Zherebtsov and Ignatiev[66] (LiF–NaF–BeF_2 (15–58–27 mol%) and LiF–NaF–BeF_2 (17–58–25 mol%)) and in both cases found good agreement with the experimental data, which gave legitimacy to their approach.

Assuming that the density of the recommended fuel matrix (LiF–NaF–BeF_2 (20.6–57.9–21.5 mol%)) follows Eq. (13), we can estimate the density of the fuel with the contribution of 1.3 mol% PuF_3, using the additive law of molar volumes. For this calculation, we need to know the molar volume of pure liquid PuF_3, which, to our best knowledge, has not been determined experimentally. To derive this quantity, we assume that liquid PuF_3 has the same molar volume as CeF_3, which was obtained from the density measured by Kirshenbaum and Cahill[84] for the temperature range of 1700–2200K. For its similar chemical behavior, CeF_3 is considered as a proxy compound to the plutonium species, a consideration that is supported by the comparison of the ionic radii of Ce^{3+} and Pu^{3+}, which are nearly identical, 115 pm for Ce^{3+} and 114 pm for Pu^{3+}. The density function of pure liquid PuF_3 thus obtained is:

$$\rho(\text{kg m}^{-3}) = 9550.6 - 1.4296 T(\text{K}) \tag{14}$$

giving

$$\rho(\text{kg m}^{-3}) = 2759.9 - 0.5730 T(\text{K}) \tag{15}$$

for the fuel composition (LiF–NaF–BeF_2–PuF_3 (20.3–57.2–21.2–1.3)).

To estimate viscosity, Khokhlov *et al.*[82] applied a similar approach as in the case of density. According to their report, the input data were the experimental results of the molar viscosities of binary LiF–BeF_2, NaF–BeF_2,[73] and LiF–NaF melts.[85] The obtained temperature function of kinematic viscosity of the LiF–NaF–BeF_2 (22–56.7–21.3 mol%) composition is shown in **Fig. 19**. The same figure shows a comparison of the estimated curve with the experimental data measured by Ignatiev *et al.*[86,87] and there is a close agreement between both sets of results. The corresponding dynamic viscosity of the LiF–NaF–BeF_2 (22–56.7–21.3 mol%) composition is given in the following equation:

$$\log_{10} \eta(\text{mPa s}) = -1.0018 + (1617.4/T(\text{K})) \tag{16}$$

As this composition is very close to the recommended fuel choice, neglecting the influence of addition of a relatively small amount of PuF_3 (1.3 mol%), we recommend Eq. (16) as a viscosity function of the LiF–NaF–BeF_2–PuF_3 (20.3–57.1–21.2–1.3 mol%) fuel.

5.18.4.4.5 NaCl–UCl_3

The density and viscosity of the binary NaCl–UCl_3 system has been measured by Desyatnik *et al.*[88] for wide composition range. The results for molar volume as function of UCl_3 composition at T = 1100K are shown in **Fig. 20**. From the data presented by the authors, we have interpolated temperature function of density for the NaCl-UCl_3 (55–45 mol%) composition, corresponding to the fuel composition from **Table 4** taking into account chemical similarities of U- and Pu-trichlorides as:

$$\rho(\text{kg m}^{-3}) = 4333.6 - 0.919 T(\text{K}),$$

and similarly for viscosity as:

$$\log_{10} \eta(\text{mPa s}) = -1.2866 + \left(\frac{1762.5}{T(\text{K})}\right).$$

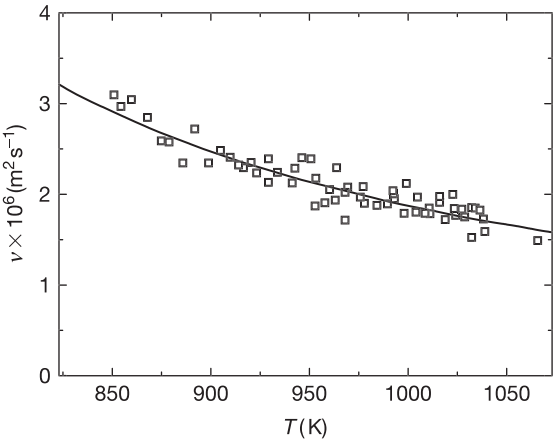

Fig. 19 Kinematic viscosity of the LiF–NaF–BeF_2 (22–56.7–21.3 mol%) melt: (—) estimated data from Khokhlov *et al.*; (□) experimental data by Ignatiev *et al.* Reproduced from Beneš, O., Konings, R.J.M., 2009. J. Fluor. Chem. 130, 22–29. Khokhlov, V., Ignatiev, V., Afonichkin, V., 2009. J. Fluor. Chem. 130, 30–37. Ignatiev, V., Merzliakov, A., Afonichkin, V., *et al.*, 2002. Proceedings of the 7th Exchange Meeting on Actinide and Fission Product Partitioning Trans-Mutation, September 9–14, 2002. Jeju, Korea. pp. 581–590. Ignatiev, V., Grebenkine, K., Subbotin, V., *et al.*, 2003. Proceedings of the International Symposium on Ionic Liquids. June 26–28, 2003. Carry le Rouet, France. pp. 203–310.

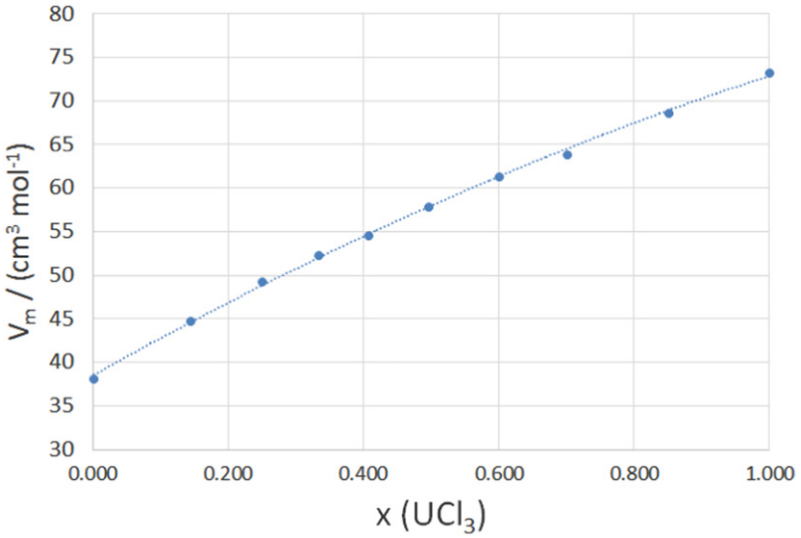

Fig. 20 Molar volume of the NaCl–UCl_3 system at 1100K. The experimental data are taken from Desyatnik *et al.* Reproduced from Desyatnik, V.N., Katyshev, S.F., Raspopin, S.P., Chervinskij, Y.F., 1975. At. Energiya 39 (1), 70–72.

5.18.4.4.6 NaF–$NaBF_4$

The density of NaF–$NaBF_4$ (8–92 mol%) was measured by Cantor[70] from 673 to 864K. The results can be represented by the equation:

$$\rho(\mathrm{kg\ m^{-3}}) = 2446.3 - 0.711T(\mathrm{K}) \tag{17}$$

The viscosity of NaF–$NaBF_4$ (8–92 mol%) was measured by Cantor[70] from 682 to 810K. The results can be represented by the equation:

$$\eta(\mathrm{mPa\ s}) = 0.0877 \exp(2240/T(\mathrm{K})) \tag{18}$$

5.18.4.4.7 LiF–NaF–KF

The density of the eutectic melt of the LiF–NaF–KF system has been measured by Chrenková *et al.*[89] for the temperature range of 940–1170K. The exact composition of the LiF–NaF–KF melt measured in their study was $x(\mathrm{LiF}) = 0.465$, $x(\mathrm{NaF}) = 0.115$, and $x(\mathrm{KF}) = 0.420$, thus corresponding to the eutectic composition found by Bergmann and Dergunov.[61] The density as a function of temperature of the eutectic composition has also been reported by Powers *et al.*[81] for an unspecified temperature range. As shown

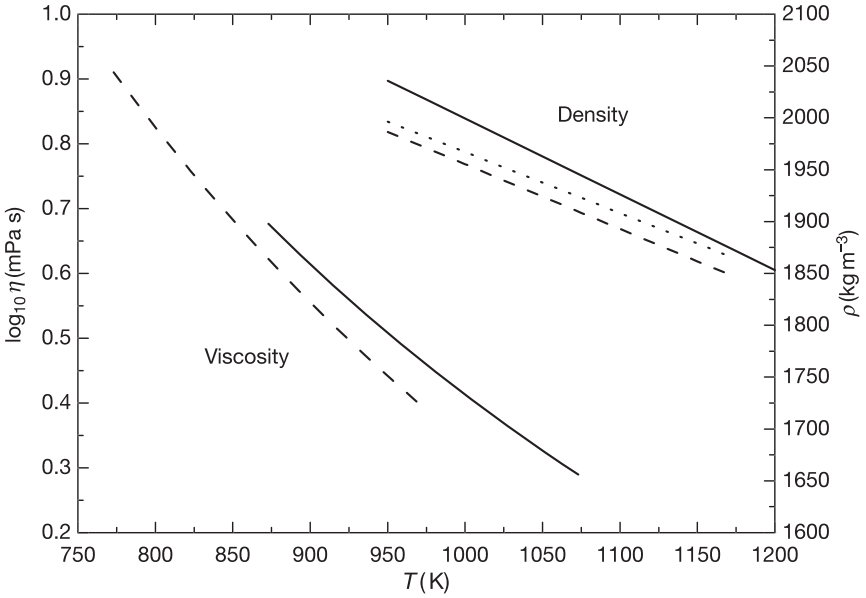

Fig. 21 Viscosity and density functions of temperature reported by Chrenková *et al.* (– – –) and Powers *et al.* (– –). For comparison, the ideal density behavior is represented by a dotted line. Reproduced from Beneš, O., Konings, R.J.M., 2009. J. Fluor. Chem. 130, 22–29. Chrenková, M., Daneïk, V., Vasiljev, R., *et al.*, 2003. J. Mol. Liq. 102, 213–226. Powers, W.D., Cohen, S.I., Greene, N.D., 1963. Nucl. Sci. Eng. 71, 200–211.

in Fig. 21, the data by Chrenková *et al.* and Powers *et al.* differ significantly. The results of Chrenková *et al.* are close to the density that is calculated assuming ideal behavior and the curve has almost the same slope, which is consistent with our observations that most of these fluoride systems are ideal. For this reason, we recommend the data by Chrenková *et al.*:

$$\rho\left(\text{kg m}^{-3}\right) = 2579.3 - 0.6240T(\text{K}) \tag{19}$$

The viscosity of the eutectic melt of the LiF–NaF–KF system has been measured by Chrenková *et al.*[89] for the temperature range of 773–973K and Powers *et al.*[81] for the temperature range of 873–1073K. The comparison between the data by Chrenková *et al.* and by Powers *et al.* is shown in Fig. 21. The data by Chrenková *et al.* have been selected:

$$\log_{10}\eta(\text{mPa s}) = -1.6044 + 1944/T(\text{K}) \tag{20}$$

5.18.4.5 Heat Capacity and Thermal Conductivity

5.18.4.5.1 $LiF–BeF_2$

The heat capacity of liquid LiF–BeF_2 (66–34 mol%) has been measured by Hoffman and Cooke (as cited in Cantor *et al.*[90]), and Douglas and Payne,[91] who obtained 2.41 J K^{-1} g^{-1} (unknown temperature range) and 2.37 J K^{-1} g^{-1} (773–873K), respectively. The value C_p(LiF–BeF_2 (66–34 mol%)) = 2.39 J K^{-1} g^{-1} has been selected.

The thermal conductivity of LiF–BeF_2 (66–34 mol%) has been measured by Cooke (as reported in Cantor *et al.*[90]) to be 1.0 W m^{-1} K^{-1}, independent of the temperature. Later on, Cooke *et al.*[92] reported more detailed results, indicating that the thermal conductivity increases slightly, from λ = 1.0 W m^{-1} K^{-1} at 923K, to about 1.2 W m^{-1} K^{-1} between 1023 and 1133K. Kato *et al.*[93] measured the thermal diffusivity of the compositions 66–34 mol% and 53–47 mol%. From their results, we calculate 1.1 W m^{-1} K^{-1} for the 66–34 mol% composition, which is in good agreement with Cooke's results, and we recommend λ (LiF–BeF_2 (66 – 34)) = 1.1 W m^{-1} K^{-1}.

5.18.4.5.2 $LiF–AnF_4$

To our best knowledge, heat capacity or thermal conductivity have not been measured for the LiF–ThF_4 system. We have estimated the heat capacity of the LiF–ThF_4 (78–22 mol%) composition on the basis of the comparison between the ideal heat capacity and the measured data from other fluoride systems taken from Powers *et al.*[81] The average positive deviation from the ideal behavior has been found to be 11%. If we combine this difference with the ideal heat capacity of the LiF–ThF_4 (78–22 mol%) composition, we obtain our suggested value: C_p = 1.0 J g^{-1} K^{-1}.

There are not enough data to accurately estimate the thermal conductivity of the LiF–ThF_4 (78–22 mol%) composition; however, we suggest that the value be slightly higher than the value of the LiF–BeF_2 (66–34 mol%) composition and close to the value for LiF–BeF_2–ThF_4 (71.7–16–12.3 mol%) composition, which was derived for T = 1023K (see Section 5.18.4.5.3). Our suggested value for LiF–ThF_4 (78–22 mol%) composition is $\lambda = \sim 1.5$ W m^{-1} K^{-1}.

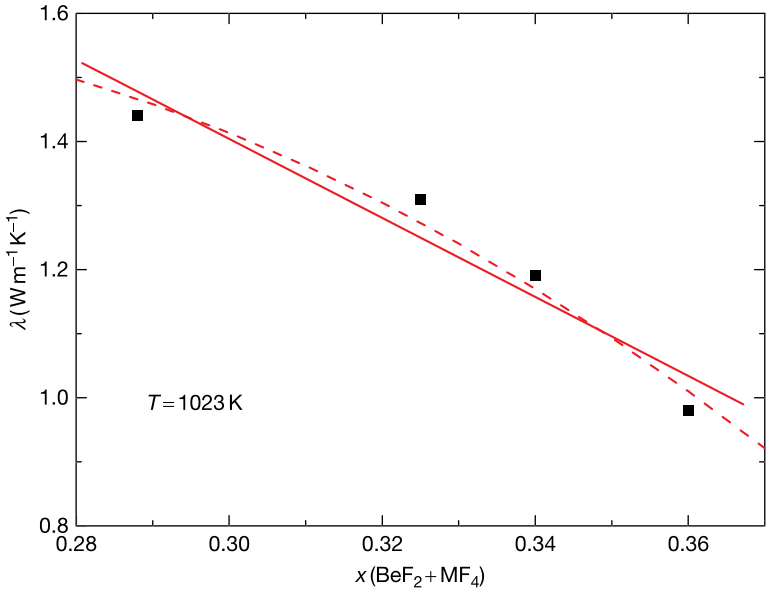

Fig. 22 Extrapolation of the thermal conductivity of the LiF–BeF_2–ThF_4 (71.7–16.0–12.3 mol%) composition at $T=1023$K. (– –) linear fit; (– – –) polynomial fit. (■) Experimental data from Cooke *et al.* and Araki and Kato. Reproduced from Beneš, O., Konings, R.J.M., 2009. J. Fluor. Chem. 30, 22–29. Cooke, J.W., Hoffman, H.W., Keyes, J.J., 1969. Technical Report ORNL-TM-4396. Araki, N., Kato, Y., 1987. Research on Thorium Fuel, Ministry of Education. Tokyo: Science and Culture. pp. 83–86.

5.18.4.5.3 LiF–BeF_2–ThF_4

Araki and Kato[94] measured the thermal diffusivity of liquid LiF–BeF_2–ThF_4 (64–18–18 mol%), from which they derived the thermal conductivity using their heat capacity data and an estimated density. The results indicate an almost constant value in the temperature range of 850–1000K: 0.95–0.98 W m^{-1} K^{-1}. The recommended heat capacity according to Araki and Kato is $C_p=1.23$ J g^{-1} K^{-1}. Both data, heat capacity and thermal conductivity, are measured for a LiF–BeF_2–ThF_4 composition that is slightly different from the one considered in this work (71.7–16.0–12.3 mol%). Cooke *et al.*[92] reported (in graphical form only) the thermal conductivity of liquid LiF–BeF_2–ThF_4–UF_4 (67.5–20–12–0.5 mol%) for the temperature range of 800K–1150K. The data scatter around $\lambda=1.2$–1.4 W m^{-1} K^{-1}, with a suggested maximum at 973K. This result is somewhat different from that of Araki and Kato.[94] As the results for liquid LiF–BeF_2 from both groups are in good agreement, the variation probably arises from differences in BeF_2 and MF_4 content (where M=Th, U, and Zr). The results from the above-mentioned sources[92,94] indicate that in the measured composition range, the thermal conductivity decreases with increasing (BeF_2 + MF_4) content as indicated in Fig. 22. The LiF–BeF_2–ThF_4 (71.7–16.0–12.3 mol%) composition is just outside this range (x(BeF_2 + MF_4)=28.3 mol%), and linear extrapolation would suggest $\lambda=1.51$ W m^{-1} K^{-1} at $T=1023$K (solid line in Fig. 22). However, such linear extrapolation would suggest a relatively high thermal conductivity of LiF–ThF_4 (78–22 mol%). Alternatively, one could extrapolate the results in a nonlinear way (dashed line in Fig. 22). This would suggest $\lambda=1.49$ W m^{-1} K^{-1} at $T=1023$K, which is very close to previously established value. In this case, the thermal conductivity of LiF–ThF_4 (78–22 mol%) is 1.6 W m^{-1} K^{-1}, which is more realistic. For LiF–BeF_2–ThF_4 (71.7–16.0–12.3) composition we recommend:

$$\lambda = 1.5 \ \text{W m}^{-1}\ \text{K}^{-1} \tag{21}$$

The heat capacity of the quaternary LiF–BeF_2–ThF_4–UF_4 (71–16–12–1 mol%) composition, which is nearly identical to our reference selection (LiF–BeF_2–ThF_4 (71.7–16–12.3 mol%)), has been reported in Briant and Weinberg,[80] giving $C_p=1550$ J kg^{-1} K^{-1}. This value is also fairly close to the estimated value, based on the approach published by Khokhlov *et al.*[82] (discussed in the following section), which gives $C_p=1.506$ J g^{-1} K^{-1}. We select the measured value, $C_p=1.550$ J g^{-1} K^{-1}.

5.18.4.5.4 LiF–NaF–BeF_2–PuF_3

Because of the lack of experimental data on the heat capacity of the actinide-containing salts, it is difficult to properly assess the value for the LiF–NaF–BeF_2–PuF_3 (20.3–57.1–21.2–1.3 mol%) composition. However, Khokhlov *et al.*[82] recently evaluated the heat capacity of more than 30 fluoride salts and found a simple empirical dependence on the inverse molar mass (1/M) by the following equation:

$$C_p\left(\text{J K}^{-1}\ \text{g}^{-1}\right) = 0.2916 + 0.00802 \times 10^4/\text{M} \tag{22}$$

Using the above equation, the heat capacity for the fuel composition from Table 4 is calculated as 2.15 J K^{-1} g^{-1}. This value is fairly close to the experimentally determined heat capacity of the plutonium-free LiF–NaF–BeF_2 (24–53–23 mol%) composition, which was found at 2.26 J K^{-1} g^{-1}. Because this composition is similar to the fuel composition and its heat capacity is only slightly

higher than that found for the fuel composition using Eq. (22), we recommend 2.15 J K^{-1} g^{-1} as a reasonable estimate of the heat capacity.

Because of the lack of experimental data, it is difficult to assess the thermal conductivity of the complicated salt mixtures, such as plutonium-containing fuel; however, Khokhlov *et al.*[82] analyzed the experimental values of the thermal conductivity determined earlier for molten chlorides, bromides, and iodides of alkali metals and their mixtures and deduced an equation describing the experimental results within the measurement errors. The obtained equation depends only on temperature T (expressed in K) and the molar weight M of the salt mixture (expressed in g mol^{-1}) and is given by:

$$\lambda(\mathrm{W\ m^{-1}\ K^{-1}}) = -0.34 + 0.5 \times 10^{-3} T + 32.0/\mathrm{M} \tag{23}$$

Using this equation, the thermal conductivity of the LiF–NaF–BeF_2–PuF_3 (20.3–57.1–21.2–1.3) composition gives the following function of temperature:

$$\lambda(\mathrm{W\ m^{-1}\ K^{-1}}) = 0.402 + 0.5 \times 10^{-3} T \tag{24}$$

5.18.4.5.5 NaCl–UCl_3 and NaCl–$PuCl_3$

To our knowledge no experimental data on heat capacity and thermal conductivity of NaCl–UCl_3 and NaCl–$PuCl_3$ mixtures exists.

5.18.4.5.6 NaF–$NaBF_4$

The heat capacity of the NaF–$NaBF_4$ (8–92 mol%) melt has been determined by Dworkin (as mentioned in Cantor[70]) as $C_p = 1.506$ J g^{-1} K^{-1}.

The thermal conductivity of the NaF–$NaBF_4$ (8–92 mol%) melt has been reported by Cooke *et al.*[92] for the temperature range of 740–1000K. However, they have reported their results only in a graphical form without listing the exact values or equations. Thus, their data have been obtained by digital subtraction from the figure, and the temperature function of the thermal conductivity has been determined by a linear fit, giving:

$$\lambda(\mathrm{W\ m^{-1}\ K^{-1}}) = 0.66 - 2.37 \times 10^{-4} T(\mathrm{K}) \tag{25}$$

It is interesting to compare these results with those of Cantor *et al.*,[90] who reported preliminary measurements of the thermal conductivity of pure liquid $NaBF_4$, finding $\lambda = 0.51$ W m^{-1} K^{-1}, which is, on average, slightly higher than that of the NaF–$NaBF_4$ (8–92 mol%) eutectic composition.

5.18.4.5.7 LiF–NaF–KF

Powers *et al.*[81] reported the heat capacity of the LiF–NaF–KF (46.5–11.5–42 mol%) melt measured at $T = 973$K, giving $C_p = 1.88$ J g^{-1} K^{-1}. This value is significantly higher than that obtained from the ideal behavior ($C_{p,\ \mathrm{ideal}} = 1.66$ J g^{-1} K^{-1}).

The same authors measured the thermal conductivity of the eutectic composition, giving $\lambda = 4.5$ W m^{-1} K^{-1}. This value is much higher than the measurement (773–1173K) by Ewing *et al.*, $\lambda = 0.6$ W m^{-1} K^{-1}. Smirnov *et al.*[95] measured the thermal conductivity of eutectic LiF–NaF–KF (46.5–11.5–42 mol%) from 790 to 1080K and obtained $\lambda = 0.36 + 5.6 \times 10^{-4} T$ (K) W m^{-1} K^{-1}, giving 0.8 W m^{-1} K^{-1} at $T = 773$K. Kato *et al.*[93] measured the thermal diffusivity of LiF–NaF–KF (46.5–11.5–42 mol%) in the temperature range of 730–823K and obtained $a = 7.6 \times 10^{-4} + 6.3 \times 10^{-7} T$ (K) m^2 h^{-1}, which yields 0.8 W m^{-1} K^{-1} at $T = 773$K when combined with the selected heat capacity and density values. We thus recommend:

$$\lambda(\mathrm{W\ m^{-1}\ K^{-1}}) = 0.36 + 5.6 \times 10^{-4} T(\mathrm{K}) \tag{26}$$

5.18.4.6 Vapor Pressure

5.18.4.6.1 LiF–BeF_2

According to the thermodynamic data taken from Beneš and Konings,[33] the vapor pressure of the LiF–BeF_2 (66–34 mol%) composition has been calculated for the temperature range between 823 and 1473K, which covers the typical operating temperature range of the MSR and also describes the vapor pressure at high temperature in order to simulate the fuel behavior during accidental conditions. The result is given in the equation below:

$$\log_{10} p(\mathrm{Pa}) = 11.914 - 13,003/T(\mathrm{K}) \tag{27}$$

5.18.4.6.2 LiF–AnF_4

Vapor pressure of the LiF-ThF_4 system has been recently measured using a Knudsen Effusion Mass Spectrometry by Capelli *et al.*,[96] who determined the total and partial vapor pressures of four different LiF-ThF_4 intermediate mixtures for the temperature range 1122–1443K. The results are given in **Fig. 23** and among the measured mixtures is the LiF-ThF_4 (80.0 – 20.0 mol%) composition, which is very close to the 78–22 composition from **Table 4**. The following equation for the total vapor pressure of the LiF-ThF_4 (80.0–20.0 mol%) composition was derived:

$$\log_{10}(p/Pa) = 10.069 - 11299/(T/K) \tag{28}$$

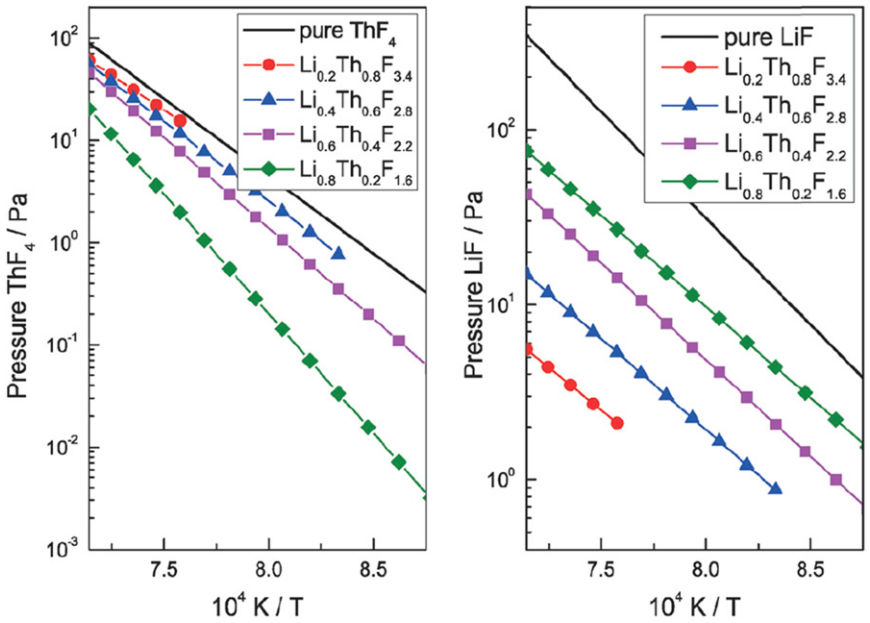

Fig. 23 Left graph: Comparison between the LiF vapor pressure (monomer) for the pure LiF liquid phase and for the $Li_xTh_{1-x}F_{4-3x}$ liquid solution. Right graph: Comparison between the ThF_4 vapor pressure for the pure ThF_4 liquid phase and for the $Li_xTh_{1-x}F_{4-3x}$ liquid solution. Reproduced from Capelli, E., Beneš, O., Colle, J.-Y., Konings, R.J.M., 2015. Phys. Chem. Chem. Phys. 17, 30110.

Recently, vapor pressure measurement of the LiF–ThF_4–UF_4 (77.5–20.0–2.5 mol%) MSFR fuel composition has been measured using the Knudsen effusion technique by Tosolin *et al.*[97] giving the following equation for the total vapor pressure:

$$\log_{10}(p/Pa) = 10.929 - 12280/\left(\frac{T}{K}\right) \tag{29}$$

valid for the temperature range 1100–1200K. The extrapolated boiling point of the LiF–ThF_4–UF_4 (77.5–20.0–2.5 mol%) fuel composition was assessed as 2019K, in a very good agreement with the thermodynamic assessment of the LiF–ThF_4–UF_4 system published by Capelli *et al.*,[98] which suggests 2021K.

Tosolin *et al.*[99] measured vapor pressure of the LiF–ThF_4–UF_4–PuF_3 (77.5–6.6–12.3–3.6 mol%) composition and from the obtained results extrapolated the boiling point as 1908 ± 77K.

5.18.4.6.3 LiF–BeF_2–ThF_4

According to the thermodynamic data by van der Meer *et al.*,[38] the vapor pressure of the LiF–BeF_2–ThF_4 (71.7–16.0–12.3 mol%) composition has been calculated for the temperature range of 823–1473K and the obtained result is shown in the following equation:

$$\log_{10} p(\mathrm{Pa}) = 11.158 - 10,790.5/T(\mathrm{K}) \tag{30}$$

The data correlate very well with the more recent assessment by Capelli *et al.*[48] and the calculated boiling temperature of the LiF–BeF_2–ThF_4 (71.7–16.0–12.3 mol%) composition is $T = 1744$K.

5.18.4.6.4 LiF–NaF–BeF_2–AnF_3

In the study by Beneš and Konings,[33] the vapor pressure of the potential fuel composition (LiF–NaF–BeF_2–PuF_3 (20.3–57.1–21.2–1.3 mol%)) has been calculated, and the results are reported in **Fig. 24**, where the total vapor pressure is highlighted by a bold curve, whereas the most volatile species are reported by thin lines. The graph does not include Pu containing species because even the most volatile among these, PuF_4, has a much lower pressure than the species reported, and therefore they have been excluded from the figure. The total vapor pressure is represented by the following equation:

$$\log_{10} p(\mathrm{Pa}) = 11.6509 - 12,827/T(\mathrm{K}) \tag{31}$$

which gives $p = 0.001$ Pa and $p = 0.046$ Pa at the designed inlet temperature ($T_{inlet} = 873$K) and the outlet temperature ($T_{outlet} = 988$K) of the MOSART reactor,[66] respectively. Both values are very low, and hence the composition shift of the fuel as a consequence of the incongruent vaporization can be neglected. The calculated boiling temperature is $T = 1973$K.

5.18.4.6.5 NaF–$NaBF_4$

The vapor pressure of BF_3 in the NaF–$NaBF_4$ system has been measured by Cantor *et al.*[100] They measured the equilibrium of the BF_3 gaseous species over the melt for the composition range of 5–100 mol% $NaBF_4$ and the temperature range of 698–1473K.

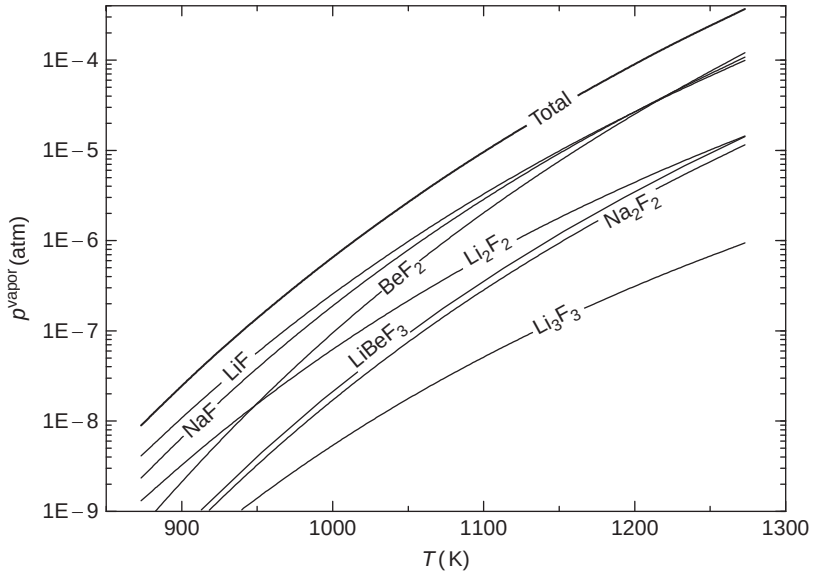

Fig. 24 Calculated vapor pressure of the x(LiF)=0.203, x(NaF)=0.571, x(BeF_2)=0.212, x(PuF_3)=0.013 potential fuel composition. Reproduced from Beneš, O., Konings, R.J.M., 2009. J. Chem. Thermodyn. 41, 1086–1095.

However, in their report they 'only' show the results for 900, 1000, and 1100K. Based on this triplet of data, the vapor pressure equation of NaF–$NaBF_4$ (8–92 mol%) has been determined, giving:

$$\log_{10} p(\text{Pa}) = 11.638 - 6550.6/T(\text{K}) \tag{32}$$

5.18.4.6.6 LiF–NaF–KF

The vapor pressure of the LiF–NaF–KF (46.5–11.5–42 mol%) composition has been calculated for the temperature range between 823 and 1473K in a study by Beneš and Konings,[65] on the basis of the thermodynamic data taken from Beneš and Konings.[64] The result is given by the equation below:

$$\log_{10} p(\text{Pa}) = 10.748 - 10,789/T(\text{K}) \tag{33}$$

5.18.4.6.7 NaCl-based systems

To our knowledge, vapor pressure measurements of mixtures of NaCl and actinide trichlorides have not been measured.

5.18.5 Role of Oxygen Impurities

In the previous section, the physicochemical properties of pure salts have been discussed. However, the behavior of these systems can be significantly affected by the presence of the oxide ion that might be resulting from contamination of the salt system; for example, the presence of reactive oxides such as H_2O can result in precipitation of the UO_2 phase.[101] Therefore, the effect of added oxide on the fuel mixture containing LiF, BeF_2, ThF_4, UF_4, and PaF_4 has been investigated in several studies,[102–109] as reported in Rosenthal *et al.*[101] who give a summary of the main conclusions from these works is given. It has been found that the solubility of the actinide dioxides in the MSBR fuel salt is low and it decreases in the order, ThO_2, PaO_2, UO_2, and PuO_2. The temperature functions of the solubilities of these oxides were estimated in the same study as follows:

$$\log_{10} Q_{ThO_2} = -2.86 - 3280/T(\text{K}) \tag{34}$$

$$\log_{10} Q_{PaO_2} = -2.86 - 4920/T(\text{K}) \tag{35}$$

$$\log_{10} Q_{UO_2} = -2.86 - 5660/T(\text{K}) \tag{36}$$

$$\log_{10} Q_{PuO_2} = -2.86 - 7100/T(\text{K}) \tag{37}$$

where

$$Q_{MO_2} = x_{M^{4+}} x_{O^{2-}}^2 \tag{38}$$

The ThF_4 concentration in the MSBR concept is equal to x=0.12, and it has been shown[101] that at such concentrations of thorium, the ThO_2 precipitation at T=773K will start for $x_{O^{2-}} \geq 8 \times 10^{-4}$.

Protactinium is produced in thorium-containing breeder fuel by neutron capture, and both tetravalent and pentavalent species of protactinium are stable. Thus, in addition to PaO_2, Pa_2O_5 can precipitate in the oxide form. As reported in Rosenthal *et al.*,[101] this oxide is very insoluble in the fluoride mixture of the MSBR composition given by:

$$\log_{10} Q_{Pa_2O_5} = 0.91 - 12,760/T(K) \tag{39}$$

in which

$$Q_{Pa_2O_2} = x_{Pa^{5+}} x_{O^{2-}}^{5/2} \tag{40}$$

Whether Pa_2O_5 will precipitate or not depends on three factors: oxide and protactinium concentrations, and the oxidation state of the fuel, which, in the MSR, is controlled by the UF_4/UF_3 ratio, as discussed in Section 5.18.8. As reported in Rosenthal *et al.*,[101] with 100 ppm Pa and 30 ppm oxide present, the UF_4/UF_3 ratio must be at least 10^5 in order to start the Pa_2O_5 precipitation. Nevertheless, such oxidizing conditions are easily avoided, as the typical UF_4/UF_3 ratio in the MSR is set to 100 (see Section 5.18.8).

Even stronger oxidizing conditions ($UF_4/UF_3 > 10^8$) are required to precipitate PuO_2, and hence this species is avoided in the MSR fuel as well.

Although the Pa_2O_5 and PuO_2 species will not be formed in the fuel salt, the other actinide dioxides UO_2, ThO_2, and PaO_2 can be formed under the redox conditions of the MSR and, due to the very low solubilities of these species in the fluoride matrix (as given by Eqs. (34)–(37)), they can easily precipitate in the solid form. Therefore, it is important to keep the fuel salt free from any oxide contamination to avoid this inadvertent event. This will certainly require some care but, as mentioned in Rosenthal *et al.*,[101] the results of the MSRE project have shown that the oxide content can be maintained at an adequately low level in order to achieve successful long-term operation of the MSR.

The role of oxygen impurities in chloride salts will be similar, but no comprehensive analysis has been published so far.

5.18.6 Electroanalytical Chemistry

Surprisingly, very little experimental work has been done on the electrochemical properties of the main ions in molten fluoride salts, but much more is known on chloride system, mainly due to the R&D program on pyrochemical reprocessing of solid oxide fuels using chloride solvents.

5.18.6.1 Electrochemical Properties of An in Molten Fluoride Salts

In comparison to molten chloride salts, studies in molten fluoride are less developed. Even though a lot of experiments were carried out in various salts (e.g., LiF–NaF, LiF–NaF–KF, LiF–CaF_2), electrochemical and thermodynamic data could not be unequivocally determined. This is mainly due to the lack of an invariable reference electrode.[110]

For the LiF–BeF_2 system, some direct measurements of the standard potentials have been made. The standard potentials of the main ions in the liquid LiF–BeF_2 (67–33 mol%) melt have been reported by Baes.[104,111,112] He has made an extensive analysis of the available literature, which is essentially based on a comparative scale as only the Be^{2+}/Be^0 couple has been measured electrochemically[113]:

$$Be(Cr) + 2HF(g) = BeF_2(sln) + H_2(g) \tag{41}$$

Using equilibrium constants, Gibbs energies of the solutes, and activity coefficients, Baes derived the values as a function of temperature as given in **Table 6**, which gives the standard potentials for the main salt carrier elements, the actinides, and some elements of structural materials. **Fig. 25** shows the electrochemical potentials calculated for $T = 1000$K.

Table 6 Standard potential in LiF–BeF_2 (66–34 mol%) relative to the HF(g)/H_2 couple, $E/V = a + bT$ (K)

Cell reaction	*a*	$b \times 10^3$
$Li^+(sln) + e^- = Li(cr)$	−3.322	0.763
$Be^{2+}(sln) + 2e^- = Be(cr)$	−2.460	0.694
$1/2F_2(g) + e^- = F^-(sln)$	+2.827	0.044
$Th^{4+}(sln) + 4e^- = Th(cr)$	−2.498	0.720
$U^{3+}(sln) + 3e^- = U(cr)$	−2.059	0.626
$U^{4+}(sln) + 4e^- = U(cr)$	−1.851	0.807
$UF_6(g) + 2e^- = U^{4+}(sln) + 6F^-(sln)$	−1.439	0.200
$Pu^{3+}(sln) + 3e^- = Pu(cr)$	−2.313	0.788
$Cr^{2+}(sln) + 2e^- = Cr(cr)$	−0.898	0.508
$Fe^{2+}(sln) + 2e^- = Fe(cr)$	−0.527	0.516
$Ni^{2+}(sln) + 2e^- = Ni(cr)$	−0.357	0.830

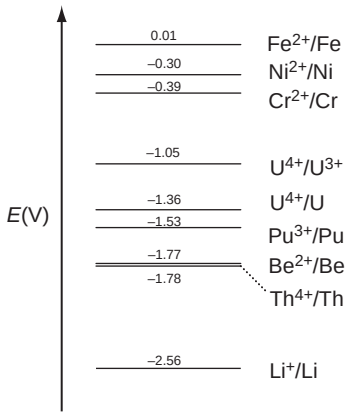

Fig. 25 Standard potential in LiF–BeF_2 (66–34 mol%) relative to the HF(g)/H_2 couple calculated at $T = 1000$K.

Table 7 Standard potential in LiF–CaF_2 (77–23 mol%) relative to the F_2/F^- pair measured by Chamelot *et al.* at $T = 1100$K

Cell reaction	E^0/V
$Li^+(sln) + 1e^- = Li(cr)$	−5.33
$Th^{4+}(sln) + 4e^- = Th(cr)$	−4.57
$Nd^{3+}(sln) + 3e^- = Nd(cr)$	−4.88
$Gd^{3+}(sln) + 3e^- = Gd(cr)$	−4.93

Note: Chamelot, P., Massot, L., Hamel, C., Nourry, C., Taxil, P., 2007. J. Nucl. Mater. 360, 64–74.

Table 8 Standard potential in LiF–CaF_2 (77–23 mol%) relative to the F_2/F^- pair measured by Hammel *et al.* at $T = 993$K

Cell reaction	E^0/V
$Li^+(sln) + 1e^- = Li(cr)$	−5.44
$U^{3+}(sln) + 3e^- = U(cr)$	−4.53
$U^{4+}(sln) + 1e^- = U^{3+}(sln)$	−3.81

Note: Hammel, C., Chamelot, P., Laplace, A., *et al.*, 2007. Electrochim. Acta 52, 3995–4003.

In a recent study, Chamelot *et al.*[114] studied the electrochemical potentials of ThF_4, NdF_3, and GdF_3 in the LiF–CaF_2 (77–23 mol%) solvent in order to demonstrate the reprocessing scheme of the molten salt fuel. The LiF–CaF_2 system has been selected in their study as it has a lower melting point compared to pure LiF. The experimental results are given in **Table 7** and show that the LiF–CaF_2 (77–23 mol%) solvent can be alternatively used to reduce Th, Nd, and Gd from this salt as the redox potentials of $M^{x+} + xe^- \rightarrow M^0$ (M = Th, Nd, Gd) reactions are more positive than in the case of the $Li^+ + e^- \rightarrow Li^0$ reaction and so are reduced prior to the solvent. These authors also concluded that the LiF–BeF_2 (67 − 33) composition, as the typical MSR carrying salt, has a much narrower electrochemical window and is not suitable for the reduction of the Th, Nd, and Gd metals.

Hammel *et al.*[115] measured the electrochemical potential of UF_4 in LiF–CaF_2 (77–23 mol%) and found UF_4 less stable than the solvent components and thus suitable for reduction from this salt. The values of the redox potentials obtained in their study are summarized in **Table 8**, showing the value for the $Li^+ + e^- \rightarrow Li^0$ reaction in fair agreement with the work of Chamelot *et al.*[114]

5.18.6.2 Electrochemistry in Chloride Media

The electrochemical and thermodynamic properties of actinides and lanthanides have been extensively studied worldwide with the main focus on the carrier salt composed of LiCl–KCl eutectic mixture, which has been selected as the main candidate for pyrochemical recovery of actinides from spent nuclear fuel.[110] For development of an electrochemical separation process, the choice of cathode material onto which the actinides are deposited is crucial. The use of reactive electrodes is very advantageous, as the actinide metals are stabilized by the formation of alloys with the cathode material and undesired sidereactions of the deposit[116] can be prevented. According to the known activity coefficients of plutonium, uranium, and cerium in different reactive metals, aluminum has been identified as the reactive electrode material enabling the highest separation factor of actinides from lanthanides.[123] The formation of An-

Table 9 Deposition potentials of selected An and FPs on solid aluminum cathode in molten LiCl–KCl eutectic

Element M^{3+}/M^0 (Al)	*Temperature [°C]*	*Deposition potential [V vs. Cl^-/Cl_2]*	*Concentration [wt%]*	*Reference*
U	450	−2.25	1.58	117,118
Np	450	−2.38	3.20	117,119
Pu	450	−2.43	1.65	117,120
Am	450	−2.48	0.46	121
Nd	460	−2.63	0.50	122
Gd	460	−2.64	1.58	123
La	460	−2.68	0.84	124

Note: Souček, P., Malmbeck, R., 2015. Pyrochemical processes for recovery of actinides from spent nuclear fuels. In: Taylor, R. (Ed.), Reprocessing and Recycling of Spent Nuclear Fuel. Oxford: Woodhead Publishing. pp. 437–456.

Al and FP-Al alloys has been studied in molten LiCl-KCl in order to determine the deposition potentials (the potential point, from which the reduction starts in the real studied system). The obtained values are summarized in **Table 9**.

5.18.7 Radiation Stability of Molten Salts

As in ceramic fuels, the fuel carrier in a MSR will be subjected to various types of radiation that can cause damage, such as α- and β-decay, γ-radiation, and neutron and fission products. But unlike ceramic fuels, a liquid does not have a lattice structure (long-range order) that can be distorted. However, attention must be given to potential radiolysis issues that are driven by ionizing radiation and consequent halide molecule decomposition.

During the MSR operation the fuel salt is maintained at high temperatures, well above the melting point, and the reverse reaction counteracts primary radiolysis events. In case of fluoride salts, radiolysis leads to the formation of fluorine gas. It has been demonstrated that, during this recombination process, F_2 reacts more rapidly with salts that have primarily lost their fluorine atoms and, thus, the F_2 buildup in the reactor is eliminated.[125] Because of the fast kinetics due to the high temperature, the recovery process is rapid and radiation damage to the salt is very small. This has been confirmed in separate experiments, using accelerators, and in in-pile tests for the ARE and MSRE projects. None of these experiments have revealed indications that the fluoride salts are unstable in radiation fields.[7,125]

As stated above, once the molten salt reactor fuel remains in molten state, i.e., during operation of the reactor, and even though the radiolysis of halide salts constantly takes place, the recombination process is very fast due to the reaction kinetics at elevated temperature and the radiolysis is no issue. In other words, at these temperatures the fluorine gas, as a product of radiolysis, does not accumulate. Nevertheless, the issue of radiolysis may become significant once the fuel gets in a rest phase, e.g., during reactor cool down due to maintenance or during final storage. Therefore, it is very important to account for this issue and application of certain mitigation processes for this radiolysis might need to be put in place. Among them is the application of external heaters which will maintain the salt (e.g., during reactor shut down) above certain threshold. As reported by Blankenship,[125] radiolytic formation of F_2 occurs in the fluoride salts at fairly low temperatures ($T < 100°C$), thus the application of external heaters is technically feasible. However, such approach might not be applicable for nuclear waste of molten salt reactor fuel and although the evolution rate of F_2 gas is somehow limited by a slow fluorine diffusion within the crystal as claimed by Blankenship, for the long term storage, this may be an issue. Therefore, for studies on the chemical conversion of halide waste into other chemical forms which are immune to radiolysis and suited for final storage in a repository are ongoing. Recent data suggest that conversion into sim-rock type forms show long-term stability needed for storage purposes.

In this context it is very important to stress that the extent of radiolysis also depends on the chemical composition of the fuel salt, thus the understanding of this phenomenon for concrete fuel salt is essential. It has been shown that e.g., fuel containing large concentrations of UF_4 will generate more free fluorine gas due to radiolysis compared to salts based on ThF_4 or PuF_3.

In case of chloride fuel, less knowledge is available about the radiation effects on fuel. However, it is known from studies[126] that gamma irradiation of rock salt (NaCl) leads to the formation of chlorine gas and colloidal sodium at temperatures between 273 and 473K, similar to fluoride salts. The issues for chloride salt will thus be similar, but details about temperature and dose dependence are needed.

5.18.8 Fission Product Behavior

The fission products that are formed during the operation of the MSR can be divided into three main groups based on their solubilities in the carrying matrix: noble gases, stable salt-soluble elements, and noble metals that are very difficult to dissolve in the salt matrix. Whether the fission product will or will not be dissolved by the salt is determined by the redox potential of the salt. Current knowledge on fission product behavior is limited to fluoride salts.

As demonstrated in the MSRE project, the redox potential of the salt is controlled by the UF_4/UF_3 ratio in such way that the corrosion of the structural material, for example, leaching of chromium (the least stable element in the Ni-based alloys, see

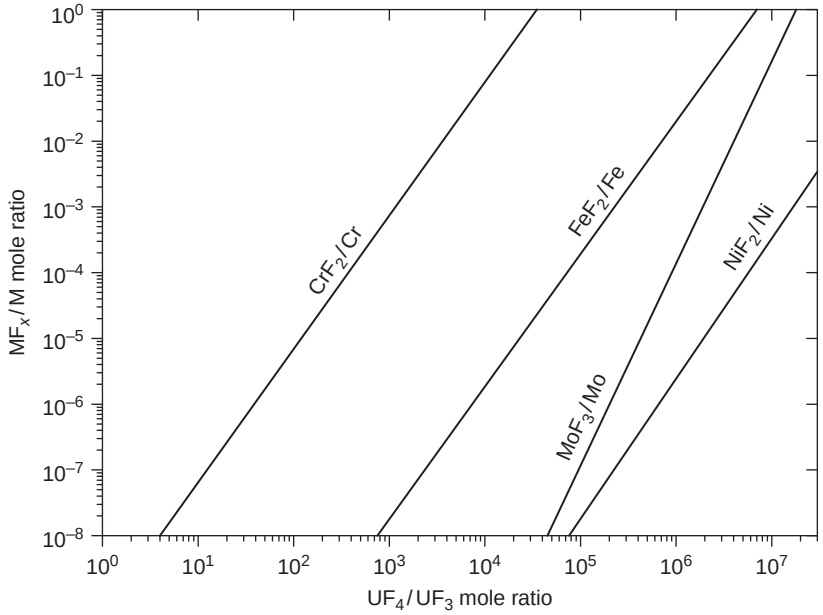

Fig. 26 Variation of equilibrium concentration of structural metal fluorides as a function of the UF_4/UF_3 ratio in a molten salt reactor fuel. Reproduced from Rosenthal, M.W., Haubenreich, P.N., Briggs, R.B., 1972. Technical Report ORNL-4812.

Section 5.18.9) from the Hastelloy-N,[104] is inhibited. As reported by Rosenthal *et al.*,[101] the UF_4/UF_3 ratio in the MSRE was ~ 100. It is shown in **Fig. 26** that at this concentration the ratio of dissolved chromium in the form of CrF_2 and its metal form is $<10^{-5}$. Taking into account that the UF_4/UF_3 ratio is set in such way not to form chromium fluoride, one can assume that fluorides that have more negative free energy of formation ΔG_f^0 according to the general reaction:

$xM_{metal} + \gamma F_{2gas} \rightarrow xMF_{2y}$ ΔG_f^0 will dissolve in the fuel, whereas the ones that have higher ΔG_f^0 of the above given reaction will precipitate in the form of insoluble metals.

During the operation of the MSR, free fluorine is formed from the fission processes. This fluorine preferably reacts with UF_3, increasing the UF_4/UF_3 ratio and thus changing the redox potential of the salt. This will certainly increase the corrosion rate of the structural material; therefore, the UF_3 concentration must be readjusted. This is achieved by adding small amounts of pure metals, for example, beryllium, which absorb fluorine. In the MSRE, a beryllium rod was kept immersed in the salt until the UF_3 concentration reached the correct value. On the other hand, as discussed in Section 5.18.9, too high a content of UF_3 is not allowed in the MSR as it can corrode graphite or other structural components. Hence, one must be able to control the redox potential of the salt in the other direction also to achieve more oxidizing conditions, and thus increasing the UF_4/UF_3 ratio. In the MSRE, this was done by adding NiF_2 into the fuel. At the redox conditions of the MSR, NiF_2 decomposes to metallic nickel and fluorine, which then reacts with UF_3 forming more UF_4.

5.18.8.1 Noble Gases

The solubility of inert gases in molten fluoride salts has been measured by a limited number of authors. Grimes *et al.*[127] measured the solubility of He, Ne, Ar, and Xe in NaF–ZrF_4 (53–47 mol%) and NaF–ZrF_4–UF_4 (50–46–4 mol%); Blander *et al.*[128] measured the solubility of He, Ne, and Ar in LiF–NaF–KF eutectic; and Watson *et al.*[129] measured the solubility of He, Ne, Ar, and Xe in LiF–BeF_2 (64–36 mol%).

These studies all show that the solubilities increase linearly with gas pressure and temperature and decrease with increasing atomic weight of the gas atom. All experimental data confirm that the solubility of these noble gases follows Henry's Law, which says that in very dilute solutions, the pressure is proportional to the mole fraction:

$$p_i = k_H x_i \tag{43}$$

The proportionality factors k_H derived from the experiments for LiF–BeF_2 (64–36 mol%) are plotted in **Fig. 27** as a function of the reciprocal temperature and listed in **Table 10**.

As is obvious from the table and the figure, the noble gases are only slightly soluble in molten salts. They can be removed from the fuel by sparging with helium to an off-gas system. As reported in Engel *et al.*,[130] it was demonstrated during the operation of the MSRE that about 80% of ^{135}Xe, the highest noble gas neutron poison was removed using this method. It was observed in Rosenthal *et al.*[101] that no compounds are formed with noble metals under the MSR conditions, which prevents the noble metals from being chemically bonded to the fuel salt.

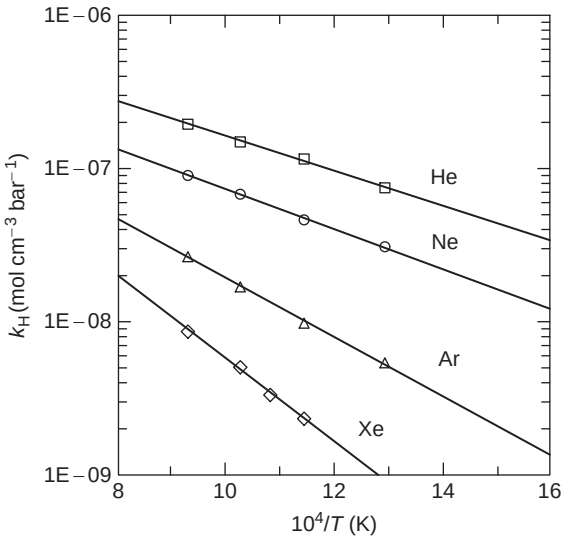

Fig. 27 The Henry's constant k_H of noble gases as a function of the reciprocal temperature in molten LiF–BeF_2 (64–36 mol%). Reproduced from Watson, G.M., Evans, R.B., Grimes, W.R., Smith, N.V., 1962. J. Chem. Eng. Data 7, 285–287.

Table 10 The Henry's constant k_H of noble gases in molten LiF–BeF_2 (64–36 mol%) as a function of the temperature

T (K)	*Solubility ($\times 10^8$ mol cm^{-3})*			
	He	*Ne*	*Ar*	*Xe*
773	7.49 ± 0.07	3.09 ± 0.09	0.54 ± 0.02	
873	11.55 ± 0.39	4.63 ± 0.01	0.98 ± 0.02	0.233 ± 0.002
923				0.333 ± 0.011
973	14.93 ± 0.42	6.80 ± 0.09	1.69 ± 0.10	0.505 ± 0.020
1073	19.48 ± 0.01	9.01 ± 0.15	2.66 ± 0.06	0.863 ± 0.021

Source: Watson, G.M., Evans, R.B., Grimes, W.R., Smith, N.V., J. Chem. Eng. Data 7, 285–287.

5.18.8.2 Salt-Soluble Fission Products

Alkali metals (mainly Rb, Cs), alkali-earth (mainly Sr, Ba), the lanthanides, and Y with Zr, all form stable fluorides and are soluble in the fuel salt. Hence, they are expected to be found completely dissolved in the fuel, except for the ones that have noble gas precursors with relatively long half-lives and these are removed prior to their decay by the off-gas system. It was demonstrated experimentally that these isotopes with noble gas precursors (^{89}Sr and ^{137}Cs) show ratios to the calculated inventory that are significantly lower than those without, which generally scatter around 1.0.[101] Although an online cleanup will be made for the MSR fuel, some of the fission products from this group will remain dissolved in the salt during the lifetime of the reactor. However, as reported, for example, in the MSR FUJI concept,[15] for a thermal spectrum reactor, the accumulation of these fission products will be relatively small, within the tenths of wt%, mostly represented by Zr and lanthanides, followed by cesium. Such low concentrations will only negligibly affect the fuel properties, as demonstrated in a recent study by Beneš and Konings.[39]

5.18.8.3 Insoluble Fission Products

This group of fission products is mostly represented by noble metals that are more thermodynamically stable to oxidation than chromium in the structural alloy, at the redox conditions maintained in the MSR. Therefore, they are expected to be found in the fuel in the metal form. Noble metals that will accumulate in the MSR in significant amounts are isotopes of Nb, Mo, Tc, Ru, Ag, Sb, and Pd. As confirmed by the MSRE,[8,101,131] selenium and tellurium are also expected to be present in the reactor circuit in metal form; however, as discussed in Section 5.18.9, the reduction of tellurium in the salt to telluride can be achieved by increasing the UF_3/UF_4 ratio to about 0.05.[132]

As the noble metals are insoluble in the fluoride salt, it is important to understand the state of these fission products within the fuel circuit. Based on the MSRE samples,[132] some metallic particles were found in the helium sparge gas, some were deposited on the metallic surfaces of the primary circuit, and a smaller fraction was found deposited on the graphite specimens. The aim is to

avoid the precipitation of these metallic fission products on the structural materials as the deposited material contributes to the heat generation from its decay even after the reactor shutdown, decreasing the overall safety of the MSR. Furthermore, the deposits on the graphite specimens in the case of thermal reactors absorb neutrons during the operation and lead to lower efficiency of the reactor. One way of avoiding this detrimental precipitation is to remove the insoluble fission products by helium bubbling before they interact with the structural materials.

5.18.8.4 Iodine

A separate section is devoted here to iodine, as it does not fit into either of the above-mentioned categories. At the redox conditions of the MSR, iodine is stabilized in the fuel salt in the form of the I^- anion, but as the iodide is not well miscible with fluoride (or chloride) solvents, it might stay undissolved in the fuel, as demonstrated in a thermodynamic study by Capelli *et al.*[133]

From the thermodynamic point of view, it would be necessary to have a UF_4/UF_3 ratio of at least 10^4 in order to strip 0.1% of I^- as I_2 in the off-gas system.[131] Such conditions are highly oxidizing and are not allowed as the rate of chromium leaching from the Hastelloy-N would be too high. Based on the MSRE observations, the experimentally obtained inventories of iodine found in the fuel salt mostly ranged somewhere between 30% and 60% of the calculated ones. Why such relatively small amounts were observed is not clear, but one of the possible explanations is that the ^{131}Te precursor of iodine with a half-life of 25 min had been stripped from the fuel before it decayed to ^{131}I or deposited on the surfaces of the reactor vessels.[131]

5.18.9 the Effect of Corrosion Reactions on the Fuel Behavior

Corrosion of the structural materials of the reactor by the molten salt may affect the chemistry and redox conditions of the fuel. The corrosion process to be considered in this context is the oxidation of metals in the alloy phase and their dissolution in the salt phase. As a result of the MSRE experience, knowledge of corrosion behavior of fluoride salts is much better developed than for chloride salts, and therefore this section dealts with the former only.

From the thermodynamic point of view, Cr is the least stable element in relevant Ni-based alloys such as Hastelloy-N, as can be seen in Fig. 28. It is not useful to apply a protective coating of, for example, an oxide layer on the structural material for the two following reasons: although some oxides are relatively insoluble in the fluoride melt, most are readily dissolved, and all rapidly recrystallize.[132] Therefore, the clean metal must withstand the corrosive attack of the salt.

As discussed by Briggs,[134] three principal corrosion processes can be distinguished:

(1) Reactions due to oxides on the metal: Oxide films on the surface of the alloy can be attacked by the fluoride melt:

$$Cr_2O_3 + 3BeF_2(salt) = 2CrF_3(salt) + 3BeO$$

$$FeO + BeF_2(salt) = FeF_2(salt) + BeO$$

The formed oxides are of little consequence as long as they do not contain fissile elements, but the formed fluorides will act as oxidants of Cr in the alloy.

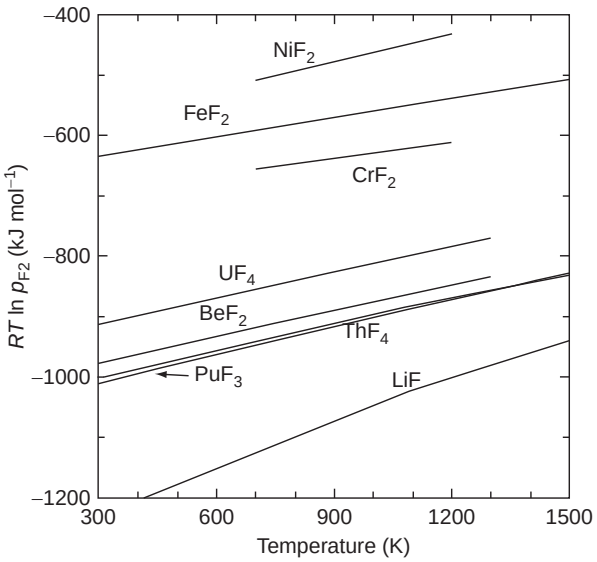

Fig. 28 The stability of selected metal fluorides.

(2) Reactions with dissolved impurities: In addition to impurities generated by reactions with oxides, impurities may result from incomplete removal of HF or of easily reducible fluorides during the salt purification, which is done by successive reactions with HF–H_2 and H_2. In this case, the following reactions should be considered:

$$Cr(alloy) + 2HF(salt) = CrF_2(salt) + H_2(g)$$

$$Cr(alloy) + FeF_2(salt) = CrF_2(salt) + Fe$$

(3) Reactions with necessary constituents of the melt: The oxidation reaction of alloy components with UF_4 has been suggested by Koger[135] to play an important role in the corrosion:

$$Cr(alloy) + 2UF_4(salt) = CrF_2(salt) + 2UF_3(salt)$$

Eq. (44) will define/buffer the electrochemical (redox) potential of the salt via the UF_4/UF_3 ratio:

$$K_{47} = \frac{a_{CrF_2} a^2_{UF_3}}{a_{Cr} a^2_{UF_4}} = \frac{(\gamma x)_{CrF_2} (\gamma x)^2_{UF_3}}{(\gamma x)_{Cr} (\gamma x)^2_{UF_4}} \tag{44}$$

in which a is the activity and γ is the activity coefficient. The redox potential is therefore a measure of chemical reactivity of the fuel salt. The more negative it is, the lower the activity of fluorine, and the more reductive the salt is, leading to a less corrosive environment. On the contrary, the more positive the redox potential, the more oxidative and corrosive the salt will be. Since most of the MSR concepts consider UF_4 as one of the major actinoid-bearing constituents of the salt, the most suitable way to control the redox potential is to regulate the concentrations, respectively activities, of the dissolved uranium (IV) and (III) ions, the so called "U(IV)/U(III) redox buffer". The higher concentration, respectively the activity of U^{3+} ions, the more negative the redox potential of the fuel salt will be. At the same time, with higher U(III) ion content, the less corrosive against the construction materials the salt will be.

During the MSR reactor operation, fluorine gas is produced by the fission reaction of UF_4, during which fission products with an average of the total valence less than four are formed according to the simplified equation (Eq. (45)). Depending on the value, the fluorine potential (or partial pressure of fluorine gas in equilibrium with the salt) can oxidize UF_3 to UF_4, according to Eq. (46), which leads to an increase of the U(IV)/U(III) concentration ratio, increase of the redox potential of the fuel salt and to the reactor vessel corrosion.[136,137]

$$UF_4 + n \rightarrow Kr_{(g)} + LnF_3 + \tfrac{1}{2}F_{2(g)} \tag{45}$$

$$UF_3 + \tfrac{1}{2}F_{2(g)} \rightarrow UF_4 \tag{46}$$

As the most reactive element of the considered structural materials based on Ni-based alloys is chromium, the main corrosion reaction would be oxidation of chromium by uranium (IV) ions:

$$2UF_4 + Cr \rightarrow 2UF_3 + CrF_2 \tag{47}$$

Briggs[134] showed that, based on reasonable estimations of the activity coefficients for the above reaction, the equilibrium concentration of CrF_2 is of the order of 130–300 ppm for a fuel with 1% UF_4 in contact with Hastelloy-N.

The equilibrium concentration of Cr in the MSRE fuel salt was found to be (72 ± 8) ppm, which after variation of the operation temperature increased to 85 ppm.[138] This is lower than the approximate equilibrium concentration. Also, the observed rates of corrosion in the MSRE have been significantly lower than predicted from thermodynamic data and diffusion theory. It has been postulated that one of the principal reasons for the unexpectedly low values observed is that the metal surfaces of the fuel circuit have been covered with a film of the noble-metal fission products Nb, Mo, Tc, and Ru about 10 Å thick.[138] Such low Cr concentrations in the fuel will not have a large impact on the properties of the fuel salt.

To inhibit corrosion, control of the U(IV)/U(III) concentration ratio is needed and if the ratio increases over 100, part of the UF_4 content must be reduced back to UF_3. It can be done chemically by introducing a suitable metal as a reductant. The metal must be chemically reducing enough to reduce U^{4+} ions to U^{3+}, and at the same time, it should not form a product introducing new chemical species to the fuel salt. In practice, suitable metals include Be (if BeF_2 is part of the fuel matrix) or U, which cations are already present in the fuel salt. The reduction is described by the chemical equilibrium using the example of Be metal as the reductant:

$$2UF_4 + Be \rightarrow 2UF_3 + BeF_2 \tag{48}$$

A special paragraph must be devoted to the influence of the fission product tellurium on the corrosion aspects of the fuel salt. When it is present in the metallic form in the fuel, it corrodes Ni-based alloys and embrittles its surface grain boundaries. This embrittlement is a vital issue to consider because, in the long term, it can result in cracking of the structural materials. As reported in Keiser,[139,105] an investigation using chromium telluride as tellurium source was carried out in order to understand the mechanism of this type of corrosion. It was concluded that the intergranular embrittlement produced in Hastelloy-N can be significantly reduced by adding 1–2 wt% of niobium into the Hastelloy-N. Another way to suppress the corrosion rate is by increasing the reducing conditions of the fuel, which is done by the increase of the UF_3/UF_4 ratio (done in the MSRE by adding Be metal into the fuel). At such conditions, tellurium would be present as Te^{2-} anion rather than in an 'oxidized' metallic form, and this is less aggressive against the nickel-based alloys. On the other hand, one must be cautious because setting the UF_3/UF_4 ratio

too high will result in some parasitic reactions of the UF_3 with graphite (only in case of thermal-moderated reactor) and possibly with other materials within the primary reactor circuit.[101]

Recently, a review study on corrosion of molten salts has been published by Zhang *et al.*,[140] which we refer to for useful information.

5.18.10 Summary and Future Work

The MSR is a very promising concept for the future needs of nuclear energy. It can be designed as a thermal (graphite-moderated) or non-moderated breeder reactor that produces more fuel from ^{232}Th than it consumes, or as an actinide burner to manage the plutonium and the long-lived minor actinides (Np, Am, Cm) contained in significant amounts in the nuclear waste coming from current nuclear power plants. For a thermal spectrum reactor, the ideal candidate for the fuel matrix is a mixture of ^{7}LiF and BeF_2 because of its very low neutron capture cross-section; for the non-moderated spectrum, other fluorides or chlorides, for example, NaF or NaCl, can be considered.

A critical review of physicochemical properties of the primary fuel choices of various MSR designs (see **Table 2**) has been done in Section 5.18.4. From the evaluated data, we can conclude the following:

The thermodynamic description of the fuel systems is available and, based on these results, the liquidus temperatures, vapor pressures, and the solubility of actinide fluorides in the fuel solvent can be adequately derived. However, the addition of other matrix components must be investigated in order to decrease the melting temperature of the non-moderated MSR fuel.

The density and the derived molar volume of most binary liquid systems can be described in terms of ideal mixtures, which means that the density can be calculated by linear interpolation of the molar volumes of the end members.

The viscosity of fluoride systems shows significant nonideal mixing behavior. Notably, the binary LiF–ThF_4 system shows a strong positive deviation from ideal behavior over a wide composition range. The same has been found in the LiF–BeF_2 system. Based on these observations, it is not possible to accurately estimate the viscosity of the fluoride salts, and therefore more measurements are required.

Data on experimental heat capacity of molten fluoride systems containing actinide fluorides are generally lacking. Khokhlov *et al.*[82] derived an estimation equation that is based only on the reverse molar mass of the salt mixture. However, this method must be considered only as an approximation as it sometimes gives relatively large deviations to the experimentally determined heat capacity (e.g., pure LiF or NaF). Thus, more measurements are required in order to describe the heat capacity behavior of the liquid fluoride solutions more precisely.

Experimental data for the thermal conductivity of molten fluoride systems are generally lacking. Although Khokhlov *et al.*[82] recently derived an estimation method for this quantity on the basis of the available data for the molten chlorides, bromides, and iodides, more measurements are needed in order to justify his approach.

Attention must be also given to the corrosion of the fuel salt against the structural material. It has been reported in Sections 5.18.8 and 5.18.9 that the corrosion rate in MSRE was maintained at a very low level during the operation of the reactor, mainly by controlling the redox potential of the salt via the UF_4/UF_3 ratio and also by frequent fission product removal; however, the outlet temperature of the MSRE was 927K, which is rather low for current interests. The demand for a higher temperature regime leads to a higher corrosion rate of the Ni-based alloys (e.g., Hastelloy-N used in the MSRE); hence, new structural materials must be investigated that would withstand the attack of the salt at elevated temperatures.

Not only are the basic properties of the fresh fuel important, but also a thorough understanding of the fuel behavior under irradiation conditions is needed and in that respect many systematically driven experiments are required to: (1) understand the irradiation influence on key physico-chemical properties of the molten salt reactor fuel, (2) understand the fission product chemistry and its influence on fuel performance with respect to operational lifetime of the reactor, (3) test the material compatibility with salt under high temperature and neutron flux, (4) understand trapping of volatile fission products (e.g., fission gases) during online bubbling into off-gas system, (5) understand graphite-salt interaction in case graphite is part of the reactor core.

See also: 4.09 Material Performance in Molten Salt. 7.07 Halides of the Actinides and Fission Products Relevant for Molten Salt Reactors

References

1. US DOE Nuclear Energy Research Advisory Committee and the Generation IV International Forum, 2002. A Technology Roadmap for Generation IV Nuclear Energy Systems. Available at: https://www.gen-4.org/gif/jcms/c_40481/technology-roadmap.
2. Robertson, R.C., 1965. Technical Report ORNL-TM-728.
3. Robertson, R.C., 1971. Technical Report ORNL-4541.
4. Delpech, S., Merle-Lucotte, E., Heuer, D., *et al.*, 2009. J. Fluor. Chem. 130, 11–17.
5. Ignatiev, V., Feynberg, O., Gnidoi, I., *et al.*, 2007. Progress in Development of Li,Be,Na/F molten salt actinide recycler and transmuter concept. In: Proceedings of the ICAPP, Nice.
6. Bettis, E.S., Schroeder, R.W., Cristy, G.A., *et al.*, 1957. The aircraft reactor experiment-design and construction. Nucl. Sci. Eng. 2, 804–825.

7. Grimes, W.R., Cuneo, D.R., 1960. Reactor Handbook. vol. I. New York: Materials, Interscience, p. 425.
8. Grimes, W.R., 1970. Nucl. Appl. Technol. 8, 37.
9. MacPherson, H.G., 1985. Nucl. Sci. Eng. 90, 374.
10. Haubenreich, P.N., Engel, J.R., 1970. Nucl. Appl. Technol. 8, 118–133.
11. Smith, J., Simmons, W.E., 1974. An Assessement of a 2500 MWe Molten Chloride Salt Fast Reactor. Report AEEW - R. 956. United Kingdom Atomic Energy Authority.
12. Taube, M., Ottewitte, E.H., Ligou, J., High-Flux Fast, A., 1975. Molten Salt Reactor for the Transmutation of Caesium-137 and Strontium-90. EIR-Bericht Nr. 259. EIR.
13. Hery, M., LeCocq, A., 1983. Reacteurs a Sels Fondus. Synthese des etudesrealisees entre 1973 et1983. Synthèse Générale. Report EDF/HT/12/74/83, CEA/DGR/SEP 83/365. CEA.
14. Mourogov, A., Bokov, P.M., 2006. Energ. Convers. Manag. 47, 2761.
15. IAEA, 2007. Status of Small Reactor Designs Without On-Site Refueling. Technical Report No. IAEA-TECDOC-1536. IAEA.
16. Gruppelaar, H., Kloosterman, J.L., Konings, R.J.M., 1998. Advanced Technologies for the Reduction of Nuclear Waste. Netherlands Energy Research Foundation ECN.
17. Mathieu, L., Heuer, D., Billebaud, A., *et al.*, 2005. Proposition for a very simple thorium molten salt reactor. In: Proceedings of the Global Conference. Tsukuba, Japan.
18. Mathieu, L., *et al.*, 2006. Progr. Nucl. Energ 48, 664–679.
19. Merle-Lucotte, E., Heuer, D., Le Brun, C., *et al.*, 2006. Fast thorium molten salt reactors started with plutonium. In: Proceedings of the International Congress on Advances in Nuclear Power Plants (ICAPP). Reno, NV.
20. Merle-Lucotte, E., Heuer, D., Brun, C.L., Allibert, M., Ghetta, V., 2007. The TMSR as Actinide Burner and Thorium Breeder. Report no. LPSC 07-37. International Atomic Energy Agency.
21. Anon, 2009. GIF R&D Outlook for Generation IV Nuclear Energy Systems. GIF report.
22. Anon1, 2017. GIF Annual Report.
23. Salanne, M., Simon, C., Turq, P., 2007. J. Phys. Chem. B 111, 4678–4684.
24. Toth, L.M.; Gilpatrick, L.O., 1972. Technical Report ORNL-TM-4056.
25. Dracopolous, V., Gilbert, B., Børrensen, B., Photiadis, G.M., Papatheodorou, G.N., 1997. J. Chem. Soc. Faraday Trans. 93, 3081.
26. Dracopolous, V., Gilbert, B., Papatheodorou, G.N., 1998. J. Chem. Soc. Faraday Trans. 94, 2601.
27. Barton, C.J., 1960. J. Phys. Chem. 64, 306.
28. Rosenthal, M.W., Briggs, R.B., Kasten, P.R., 1970. Technical Report ORNL-4449.
29. Okamoto, Y., Madden, P.A., Minato, K., 2005. J. Nucl. Mater. 344, 109–114.
30. Jian-Xing, D., Wei, Z., Cui-Lan, R., *et al.*, 2018. J. Nucl. Mater. 511, 75–82.
31. Li, B., Dai, S., Jiang, D., 2019. Appl. Energy Mater. 2, 2122–2128.
32. van der Meer, J., Konings, R.J.M., Jacobs, M.H.G., Oonk, H.A.J., 2005. J. Nucl. Mater. 344, 94–99.
33. Beneš, O., Konings, R.J.M., 2009. J. Chem. Thermodyn. 41, 1086–1095.
34. Roy, D.M., Roy, R., Osborn, E.F., Am, J., 1954. Ceram. Soc. 37, 300.
35. Thoma, R.E., Insley, H., Friedman, H.A., Hebert, G.M., 1968. J. Nucl. Mater. 27, 166.
36. Romberger, K.A., Braunstein, J., Thoma, R.E., 1972. J. Phys. Chem. 76, 1154.
37. Holm, J.L., Kleppa, O.J., 1969. Inorg. Chem. 8, 207.
38. van der Meer, J.P.M., Konings, R.J.M., Hack, K., Oonk, H.A.J., 2006. Chem. Mater. 18, 510–517.
39. Beneš, O., Konings, R.J.M., 2008. J. Nucl. Mater. 377 (3), 449–457.
40. Barton, C.J., Strehlow, R.A., 1961. J. Inorg. Nucl. Chem. 18, 143–149.
41. Tosolin, A., Souček, P., Beneš, O., *et al.*, 2018. J. Nucl. Mater. 503, 171–177.
42. Barton, C.J., Redman, J.D., Strehlow, R.A., 1961. J. Inorg. Nucl. Chem 20, 45–49.
43. Thoma, R.E., Insley, H., Friedman, H.A., Weaver, C.F., 1960. J. Phys. Chem. 64, 865.
44. Thoma, R.E., Insley, H., Landau, B.S., Friedman, H.A., Grimes, W.R., 1959. J. Phys. Chem. 63, 1266.
45. Beneš, O., Beilmann, M., Konings, R.J.M., 2010. J. Nucl. Mater. 405, 186–198.
46. Capelli, E., Beneš, O., Konings, R.J.M., 2015. Trans. Am. Nucl. Soc. 112, 395–396.
47. van der Meer, J., Konings, R.J.M., Oonk, H.A.J., 2006. J. Nucl. Mater. 357, 48–57.
48. Capelli, E., Beneš, O., Konings, R.J.M., 2014. J. Nucl. Mater. 449, 111–121.
49. Barton, C.J., 1960. J. Phys. Chem. 64, 306–309.
50. Mailen, J.C., Smith, F.J., Ferris, L.M., 1971. J. Chem. Eng. Data 16, 68–74.
51. International Scientific Technical Centre, Moscow; Technical Report; ISTC Project #1606 Final Report; July 2004.
52. Ignatiev, V., Merzlyakov, A., Subbotin, V., Panov, A., Golovatov, Y., 2006. At. Energiya 101, 364–372.
53. Ignatiev, V., Feynberg, O., Smirnov, V., *et al.*, 2005. In: Proceedings of the ICENES-2005, August 21–26, 2005. Brussels, Belgium.
54. Thoma, R.E., 1975. Advances in Molten Salt Chemistry. vol. 3. New York, NY: Plenum, p. 275.
55. Beneš, O., Konings, R.J.M., 2008. J.Nucl. Mater. 375, 202–208.
56. Taube, M., 1978. Fast Reactors Using Molten Chloride Slats as Fuel. Würenlingen: Swiss Federal Institute for Reactor Research.
57. Sooby, E.S., Nelson, A.T., White, J.T., McIntyre, P.M., 2015. J. Nucl. Mater. 466, 280–285.
58. Bjorklund, C.W., Reavis, J.G., Leary, J.A., Walsh, K.A., 1959. J. Phys. Chem. 63, 1774–1777.
59. Selivanov, V.G., Stender, V.V., 1958. Russ. J. Inorg. Chem. 2, 279–282.
60. Barton, C.J., Gilpatrick, L.O., Bornmann, J.A., *et al.*, 1970. J. Inorg. Nucl. Chem 33, 337–344.
61. Bergmann, A.G., Dergunov, E.P., 1941. Dokl. Ac. Sc. URSS, 31. p. 753.
62. Sangster, J., Pelton, A.D., 1991. J. Phase Equilib. 12, 511.
63. Chartrand, P., Pelton, A.D., 2001. Metall. Trans. 32A, 1385.
64. Beneš, O., Konings, R.J.M., 2008. Comput. Coupl. Phase Diagr. Thermochem. 32, 121–128.
65. Beneš, O., Konings, R.J.M., 2009. J. Fluor. Chem 130, 22–29.
66. Zherebtsov, A.L., Ignatiev, V.V., 2006. Experimental Mock-up of Accelerator-Based Facility for Transmutation of Radioactive Waste and Conversion of Military Plutonium. ISTC Technical Report Nr. 1606, Annual Report.
67. Sood, D.D., Iyer, P.N., Prasad, R., *et al.*, 1975. Nucl. Technol. 27, 411–416.
68. Blanke, B.C., Bousquet, E.N., Curtis, M.L., Murphy, E.L., 1956. Technical Report USAEC MLM-1086.
69. Cantor, S., Ward, W.T., Moynihan, C.T., 1969. J. Chem. Phys. 50, 2874.
70. Cantor, S., 1971. Technical Report ORNL-TM-4308.
71. Cohen, S.I., Jones, T.N., 1957. Technical Report ORNL-2278.
72. Abe, Y., Kosugiyama, O., Nagashima, A., 1981. J. Nucl. Mater. 99, 173–183.
73. Desyatnik, V.N., Nechayev, A.I., Chervinskii, Y.F., 1981. Zh. Prikl. Khim. 54, 2310–2312.
74. Porter, B., Meaker, R.E., 1966. Technical Report BMI RI-6836.
75. Hill, D.G., Cantor, S., Ward, W.T., 1967. J. Inorg. Nucl. Chem. 29, 241–243.

76. Chervinskii, Y.F., Desyatnik, V.N., Nechaev, A.I., 1982. Zh. Fiz. Khim. 56, 1946–1949.
77. Desyatnik, V.N., Nechaev, A.I., Chervinskii, Y.F., 1979. Russ. J. Phys. Chem. 53, 986–988.
78. van der Meer, J., Konings, R.J.M., 2007. J. Nucl. Mater. 360, 16–24.
79. Mackenzie, J.D., 1960. J. Phys. Chem. 64, 306–309.
80. Briant, R.C., Weinberg, A.M., 1957. Nucl. Sci. Eng. 2, 797–803.
81. Powers, W.D., Cohen, S.I., Greene, N.D., 1963. Nucl. Sci. Eng. 71, 200–211.
82. Khokhlov, V., Ignatiev, V., Afonichkin, V., 2009. J. Fluor. Chem. 130, 30–37.
83. Janz, G.J., 1988. J. Phys. Chem. Ref. Data 17 (Suppl. 2), 21–309.
84. Kirshenbaum, A.D., Cahill, J.A., 1962. J. Chem. Eng. Data 7, 98–99.
85. Smirnov, M.V., Khokhlov, V.A., Antonov, A.A., 1979. Viscosity of Molten Alkali Halides and Their Binary Mixtures. Moscow: Nauka, p. 102.
86. Ignatiev, V., Merzliakov, A., Afonichkin, V., *et al.*, 2002. Proceedings of the 7th Exchange Meeting on Actinide and Fission Product Partitioning Trans-Mutation, September 9–14, 2002. Jeju, Korea. pp. 581–590.
87. Ignatiev, V., Grebenkine, K., Subbotin, V., *et al.*, 2003. Proceedings of the International Symposium on Ionic Liquids. June 26–28, 2003. Carry le Rouet, France. pp. 203–310.
88. Desyatnik, V.N., Katyshev, S.F., Raspopin, S.P., Chervinskij, Y.F., 1975. At. Energiya 39 (1), 70–72.
89. Chrenková, M., Daneĺk, V., Vasiljev, R., *et al.*, 2003. J. Mol. Liq. 102, 213–226.
90. Cantor, S., Cooke, J.W., Dworkin, A.S., *et al.*, 1968. Technical Report ORNL-TM-2316.
91. Douglas, T.B., Payne, W.H., 1969. J. Res. NBS 73A, 479.
92. Cooke, J.W., Hoffman, H.W., Keyes, J.J., 1969. Technical Report ORNL-TM-4396.
93. Kato, Y., Furukawa, K., Araki, N., Kato, Y., 1983. High Temp. High Press. 15, 191–198.
94. Araki, N., Kato, Y., 1987. Research on Thorium Fuel, Ministry of Education. Tokyo: Science and Culture, pp. 83–86.
95. Smirnov, M.V., Khokhlov, V.A., Filatov, E.F., 1987. Electrochim. Acta 32, 1019–1026.
96. Capelli, E., Beneš, O., Colle, J.-Y., Konings, R.J.M., 2015. Phys. Chem. Chem. Phys. 17 30110.
97. Tosolin, A., Beneš, O., Colle, J.-Y., *et al.*, 2018. J. Nucl. Mater. 508, 319–328.
98. Capelli, E., Beneš, O., Konings, R.J.M., 2015. J. Nucl. Mater. 462, 43–53.
99. Tosolin, A., Colle, J.-Y., Soucek, P., *et al.*, 2019. J. Nucl. Mater. 527, 151780.
100. Cantor, S., Roberts, C.E., McDuffie, H.F., 1967. Technical Report ORNL-4229.
101. Rosenthal, M.W., Haubenreich, P.N., Briggs, R.B., 1972. Technical Report ORNL-4812.
102. Bamberger, C.E., Baes Jr., C.F., 1970. J. Nucl. Mater. 35, 117.
103. Bamberger, C.E., Ross, R.G., Baes Jr., C.F., 1971. J. Inorg. Nucl. Chem. 33, 767.
104. (a) Baes, C.F., 1969. J. Nucl. Metall. 15, 617.
(b) Baes Jr., C.F., 1969. In Symposium on Reprocessing of Nuclear Fuels, Iowa State University, CONF-690801. Ames, IA. pp. 617–654.
105. Rosenthal, M.W., Briggs, R.B., Haubenreich, P.N., 1972. Technical Report ORNL-4782.
106. Rosenthal, M.W., Briggs, R.B., Haubenreich, P.N., 1971. Technical Report ORNL-4728.
107. Rosenthal, M.W., Briggs, R.B., Haubenreich, P.N., 1971. Technical Report ORNL-4676.
108. Rosenthal, M.W., Briggs, R.B., Haubenreich, P.N., 1971. Technical Report ORNL-4622.
109. Rosenthal, M.W., Briggs, R.B., Kasten, P.R., 1970. Technical Report ORNL-4548.
110. Souček, P., Malmbeck, R., 2015. Pyrochemical processes for recovery of actinides from spent nuclear fuels. In: Taylor, R. (Ed.), Reprocessing and Recycling of Spent Nuclear Fuel. Oxford: Woodhead Publishing, pp. 437–456.
111. Baes Jr., C.F., 1966. Proceedings of the Symposium on Thermodynamics. Vienna. pp. 409–433.
112. Baes Jr., C.F., 1974. J. Nucl. Mater. 51, 149–162.
113. Hitch, B.F., Baes Jr., C.F., 1969. Inorg. Chem. 8, 201.
114. Chamelot, P., Massot, L., Hamel, C., Nourry, C., Taxil, P., 2007. J. Nucl. Mater. 360, 64–74.
115. Hammel, C., Chamelot, P., Laplace, A., *et al.*, 2007. Electrochim. Acta 52, 3995–4003.
116. Serp, J., Chamelot, P., Fourcaudot, S., *et al.*, 2006. Electrochim. Acta 51 (19), 4024–4032.
117. Souček, P., Malmbeck, R., Mendes, E., Nourry, C., Glatz, J.-P., 2009. Recovery of Actinides fromSpent Nuclear Fuel by Pyrochemical Reprocessing. In: Proceedings of Global 2009. Paris, France.
118. Cassayre, L., Caravaca, C., Jardin, R., *et al.*, 2008. J. Nucl. Mater. 378, 79–85.
119. Souček, P., Malmbeck, R., Mendes, E., *et al.*, 2009. J. Nucl. Mater. 394 (1), 26–33.
120. Mendes, E., Malmbeck, R., Nourry, C., Souček, P., Glatz, J.P., 2012. J. Nucl. Mater. 420, 424–429.
121. Souček, P., 2008. Study of electroseparation process for spent nuclear fuel reprocessing using a reactive aluminium electrode in molten LiCl-KCl. In Faculty of Chemical Technology. Praha: Institute of Chemical Technology, p. 131.
122. Conocar, O., Douyere, N., Glatz, J.-P., *et al.*, 2006. Nucl. Sci. Eng. 153, 253–261.
123. Caravaca, C., Cordoba, G., 2006. Formation of Al-Gd alloy films by molten salt electrochemical process. In: Proceedings of EUCHEM 2006. Hammamet,Tunisia.
124. Serp, J., Allibert, M., Le Terrier, A., *et al.*, 2005. J. Electrochem. Soc. 152 (3), C167–C172.
125. Blankenship, F.F., 1964. Technical Report ORNL-3708.
126. Soppe, W.J., *et al.*, 1994. J. Nucl. Mater. 217, I–31.
127. Grimes, W.R., Smith, N.V., Watson, G.M., 1958. J. Phys. Chem. 62, 862–866.
128. Blander, M., Grimes, W.R., Smith, N.V., Watson, G.M., 1959. J. Phys. Chem. 63, 1164–1167.
129. Watson, G.M., Evans, R.B., Grimes, W.R., Smith, N.V., 1962. J. Chem. Eng. Data 7, 285–287.
130. Engel, J.R., Bauman, H.F., Dearing, J.F., Grimes, W.R., McCoy, J.H.E., 1979. Technical Report ORNL-TM-6415.
131. Compere, E.L., Kirslis, S.S., Bohlmann, e.g., Blankenship, F.F., Grimes, W.R., 1975. Technical Report ORNL-4865.
132. Engel, J.R., Bauman, H.F., Dearing, J.F., *et al.*, 1980. Technical Report ORNL-TM-7207.
133. Capelli, E., Beneš, O., Konings, R.J.M., 2018. J. Nucl. Mater. 501, 238–252.
134. Briggs, R.B., 1964. Technical Report ORNL-3708.
135. Koger, J.W., 1972. Technical Report ORNL-TM-4286.
136. Delpech, S., Cabet, C., Slim, C., Picard, G.S., 2010. Mater. Today 13 (12), 34–41.
137. Gibilaro, M., Massot, L., Chamelot, P., 2015. Electrochim. Acta 160, 209–213.
138. Rosenthal, M.W., Briggs, R.B., Kasten, P.R., 1968. Technical Report ORNL-4254.
139. Keiser, J.R., 1977. Technical Report ORNL-TM-6002.
140. Zhang, *et al.*, 2018. Corros. Sci. 144, 44.